Energy Conversion and Management 348 (2026) 120739

Contents lists available at ScienceDirect

Energy Conversion and Management

journal homepage: www.elsevier.com/locate/enconman

Research Paper

Electricity price-driven design and analysis of thermophotovoltaic energy storage systems

Wuyong Qu [a,1], Haoming Li [a,1], Zhiyuan Zhou [a], Guangyao Li [b], Neven Duić [c], Dongxu Ji [a,*]

[a] School of Science and Engineering, Chinese University of Hong Kong, Shenzhen 518172, China
[b] Interdisciplinary Graduate School of Engineering Sciences, Kyushu University, Fukuoka 816-8580, Japan
[c] Department of Energy, Power Engineering and Environment, Faculty of Mechanical Engineering and Naval Architecture, University of Zagreb, Ivana Lučića 5, 10002 Zagreb, Croatia

ARTICLE INFO

Keywords:
Energy storage
Thermophotovoltaic
Electricity price
Bandgap
System optimization

ABSTRACT

Thermophotovoltaic energy storage systems (TPVES) present a promising solution for large-scale electricity storage. To assess its economic feasibility and find optimal design, this study develops and experimentally validates a physics model to evaluate TPV performance across a wide range of emitter temperatures and semiconductor bandgaps. Building upon this, a multi-dimensional techno-economic model is established to identify economically optimal configurations by incorporating key technical parameters and economic factors, including the electricity price. Results indicate that the minimum levelized cost of storage (LCOS) can reach as low as 0.036 $/kWh, using a Si-based system with a 0.88 eV bandgap and an input electricity price of $0.01/kWh. However, the configurations that achieve this economic optimum do not coincide with those delivering peak efficiency or power density, highlighting the necessity of system-level optimization. Furthermore, by introducing electricity price as a variable, the study provides more insights into application strategies. Compared with 18 mainstream energy storage technologies, TPVES demonstrates competitive advantages in energy density (230–600 kWh/m^3), service life (20–25 years), and capital cost. While its round-trip efficiency is lower than that of many established battery systems, TPVES remains economically advantageous when electricity prices are below $0.035/kWh, making it particularly suitable for applications involving surplus or low-cost renewable energy. These findings offer practical guidance for the application of TPV technologies in future grid-scale energy storage scenarios.

1. Introduction

With the development of the world industry and economy, energy demand has been increasing continuously. According to the International Energy Agency report, total global final energy use has doubled in the last 50 years [1]. In order to meet this growing requirement, a large number of countries and institutions develop renewable resources, especially solar and wind energy. However, the power generation of these new energy technologies is intermittent due to its dependence on weather conditions and time of day, posing a significant challenge to the stability and regulation of complex power systems for electricity departments [2]. Additionally, the peak of supplying electricity for industries, health care, food and agriculture are different owing to time. Incorporating with energy storage systems (ESS) is a great method to solve the difficulty, which can reduce the energy waste.

According to the types of energy harnessed, ESS are broadly categorized into five major groups: electrical, electrochemical, thermal, chemical, and mechanical [3]. Among these, electrochemical ESS are the most widely studied and commercial application by research institutions and industry due to their high energy density, rapid response, and geographical flexibility [4]. However, safety risks and resource constraints remain significant challenges. Electrical ESS offer long cycle life and millisecond-level response times, yet their rapid self-discharge makes them unsuitable for long-term storage [5]. Chemical ESS offer the highest energy density and are environmentally friendly, yet face substantial challenges related to low round-trip efficiency and transportation logistics [6]. Mechanical ESS can achieve low levelized costs of electricity storage (LCOS) with grid-scale reliability, but their implementation is often constrained by geographical requirements [7]. By contrast, thermal ESS have gained significant attention in recent years due to its low cost at scale, long-term stability, and ability to

* Corresponding author.
E-mail address: jidongxu@cuhk.edu.cn (D. Ji).
[1] These authors contributed equally to this work.

https://doi.org/10.1016/j.enconman.2025.120739
Received 16 July 2025; Received in revised form 29 October 2025; Accepted 1 November 2025
Available online 9 November 2025

Nomenclature

Abbreviations

TPVES	Thermophotovoltaic energy storage
ESS	Energy storage systems
LCOS	Levelized costs of electricity storage
TPV	Thermophotovoltaic
CPE	Cost per energy capacity
CPP	Cost per power
ESS	Energy storage systems
LCOE	Levelized cost of electricity
PCM	Phase change material
Li-ion	Lithium-ion
LA	Pb-Acid
Na–S	Sodium-sulphur
NaNiCl2	Sodium nickel chloride
Ni-MH	Nickel-metal hydride
Ni–Cd	Nickel-cadmium
PSB	Polysulfide-bromine
ZnBr	Zinc-bromine
VRFB	Vanadium redox flow battery
SCES	Supercapacitor energy storage
SHES	Sensible heat energy storage
LHES	Latent heat energy storage
TCS	Thermochemical storage
CAES	Compressed air energy storage
FES	Flywheel energy storage
SMES	Superconducting magnetic storage
PHS	Pumped-hydro storage
GES	Gravity energy storage
O&M	Operation and maintenance

Variables

η_{out}	The output efficiency (%)
P_M	TPV maximum power density (W/m^2)
Q_{net}	Net thermal radiation (W/m^2)
J	TPV cell current (A/m^2)
V	TPV cell voltage (V)
J_0	Reverse saturation current density (A/m^2)
J_{ph}	The light generate current density (A/m^2)
n	The diode ideality factor
T_c	The temperature of the TPV cell (K)
R_s	The series resistance (Ω•cm^2)
R_{sh}	The shunt resistance (Ω•cm^2)
λ_c	Cut-off wavelength (nm)
I_{BB}	Spectral radiant power density(W/m^3)
VF	View factor (0–1)
EQE_λ	External quantum efficiency (%)
E_g	The bandgap of the TPV cell (eV)
T_{emit}	The temperature of TPV emitter (K)
ε	The emissivity of the emitter (0–1)
J_M	The current density at the MPPT (A/m^2)
V_M	The voltage at the MPPT (V)
r_{sub}	the sub-bandgap reflectance (0–1)
p_e	The price of input energy ($/kWh)
η_{rt}	Round-trip efficiency (%)
N_{cycle}	Charging and discharging cycles
t_c	Charging time (h)
t_d	Discharging time (h)
$CPOM$	Cost of operation and maintenance
η_{in}	Charging efficiency (%)
C_{cell}	The cost of TPV cell ($/cm^2)
r	Discount rate (%)

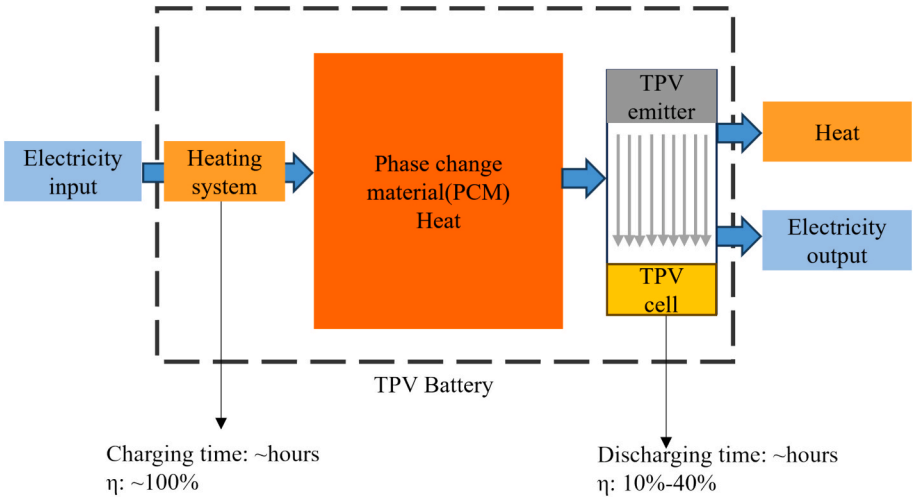

Fig. 1. The general framework of TPVES system.

provide combined heat and power [8]. Nevertheless, the conversion of thermal energy to electricity predominantly relies on technologies such as the Rankine cycle, Stirling engines, and thermoelectric generators (TEGs). The Rankine cycle is often hampered by high capital costs, a large physical footprint, and maintenance challenges associated with its numerous moving parts [9]. Stirling engines, despite their high efficiency, are limited by their bulkiness, low power density, slow dynamic response, and high cost, hindering their widespread adoption in mobile or cost-sensitive applications [10]. Meanwhile, TEGs are constrained by extremely low conversion efficiency and high costs [11]. Therefore, a novel EES based on TPV power generation is proposed as a promising new technology to overcome these limitations.

TPVES represent an electricity-to-heat-to-electricity conversion process [12], which feature static energy conversion, low-cost, modularity, and long-term storage capability, offering a promising novel approach for thermal energy storage. Recent years have witnessed significant research progress on TPV systems, demonstrating their considerable potential for future applications and success. LaPotin et al. [13]

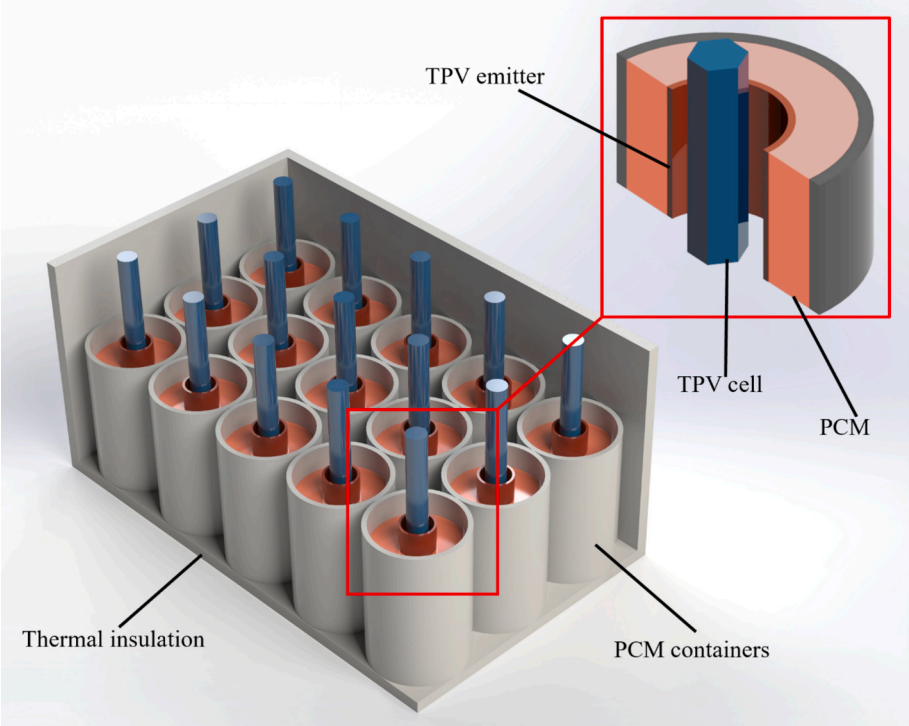

Fig. 2. A typically structure of TPVES system.

first reported the fabrication and measurement of high-bandgap tandem TPV cells achieving an efficiency exceeding 40 %. Roy-Layinde et al. [14] demonstrated that an air bridge design enables the recovery of sub-bandgap photons, allowing single-junction InGaAs TPV cells to reach 44 % efficiency under 1435 °C blackbody radiation. Amy et al. [15] proposed a novel thermal energy grid storage concept utilizing high-purity silicon as the storage material and multi-junction TPV cells as the heat engine, projecting cost per energy capacity (CPE) below 40$/kWh and cost per power (CPP) below 400$/kW. Kelsall et al. [16] presented a storage system employing graphite storage blocks and multi-junction TPV cells, predicting CPE below 20$/kWh. Additionally, spectral segmentation method utilizing both short- and long-wavelength radiation [17] and concentrated solar TPV [18] had been proposed to improve TPV application. In techno-economic analysis, assessing performance through a unified metric that evaluates the impact of efficiency and power density [19], along with calculating the levelized cost of electricity (LCOE) for various application markets [20], are widely adopted approaches. Datas et al. [21] modeled a storage system using low-cost phase change material (PCM) as the storage medium, achieving a minimum CPE of 49.5$/kWh, and compared key economic metrics with lithium-ion batteries.

While extensive research has focused on enhancing the performance and feasibility of TPV systems, several critical gaps remain. Specifically, the potential application for TPVES within real-world electricity pricing markets and the influence of cell bandgap materials on their economic feasibility remain critically underexplored. Furthermore, a comprehensive techno-economic comparison between TPVES and existing mainstream EES remains lacking. To address these gaps, this study makes three primary contributions: (1) developing a comprehensive physical and economic model to assess three distinct quality TPV system performance to select the optimal bandgap materials across varying emitter temperatures and electricity price; (2) conducting a detailed techno-economic comparison between TPVES and 18 established energy storage technologies using key metrics such as energy density, LCOS, and service life; (3) incorporates electricity price sensitivity analysis to identify the economic threshold and potential market scenarios for TPVES application.

2. Methodology

2.1. Description of TPVES

Fig. 1 depicts the general framework of TPVES system, illustrating its operational process. The system comprises electricity input, heating system, PCM, emitter and TPV cell. Electricity input typically utilizes low-cost renewable energy (e.g., solar, wind) that would be lost otherwise in low electricity consumption peak. Heating methods include ohmic, heat resistance [22], induction [23], and microwave [24]. This work employs ohmic heating due to its low cost, near-unity energy efficiency (~100 %) and uniform temperature distribution [22]. Thermal energy storage media options mainly encompass sensible heat, latent heat, and thermochemical storage materials. PCMs, representing latent heat storage, offer advantages such as high melting temperatures, high energy storage density, and low cost; examples include silicon, iron, and silicon-iron-boron alloys [25]. Compared to sensible heat materials, PCMs can provide a constant high temperature for the TPV generator, maintaining effective efficiency and power density. The emitter is typically a high-emissivity, high-temperature material approximating a blackbody. Silicon carbide (SiC), with a melting point of 2827 °C and a density of 3.21 g/cm^3, is an excellent emitter material [15]. TPV cells utilize various bandgap materials such as Ge, InAs, InGaAs, InGaSb, InAsSb, InGaAsSb, and InAsSbP [26]. The bandgap of compound semiconductors can be tuned by adjusting constituent ratios [27]; for instance, InGaAs ranges 0.5–0.74 eV and InGaAsP ranges 0.74–1.0 eV. The TPVES outputs both heat and electricity, making it suitable for dispatchable cogeneration applications [21], particularly in high-latitude regions.

Fig. 2 illustrates the schematic of the TPVES system, composed of an array of modular thermal cells. As detailed in the inset, each cell unit features a central TPV cell concentrically surrounded by a TPV emitter. This assembly is embedded within a Phase Change Material (PCM, shown in orange), which is housed in a container. The entire array is

Table 1
The key thermophysical property data of the selected materials used in TPVES [21].

Material	Density (g/cm^3)	Specific heat (J/gK)	Latent heat (J/g)	Thermal conductivity (Wm^{-1}k^{-1})	Melting temperature (℃)	Cost ($/L)	Purpose	Refs.
Si	2.33	0.98	1800	29 (solid) 60 (liquid)	1414	3.62	PCM	[29,30,31]
Fe-26Si-9B	5.39	0.95	777	30 (solid) 60 (liquid)	1157	3.62	PCM	[30]
SiC	3.21	1.26	–	–	2827	3.53	TPV emitter	[31]
Alumina fiber mat	–		–	0.26	1650 (max)	7.7	Thermal insultation	[32]
Fumed silica board	–		–	0.034	1000 (max)	2.75	Thermal insultation	[32]

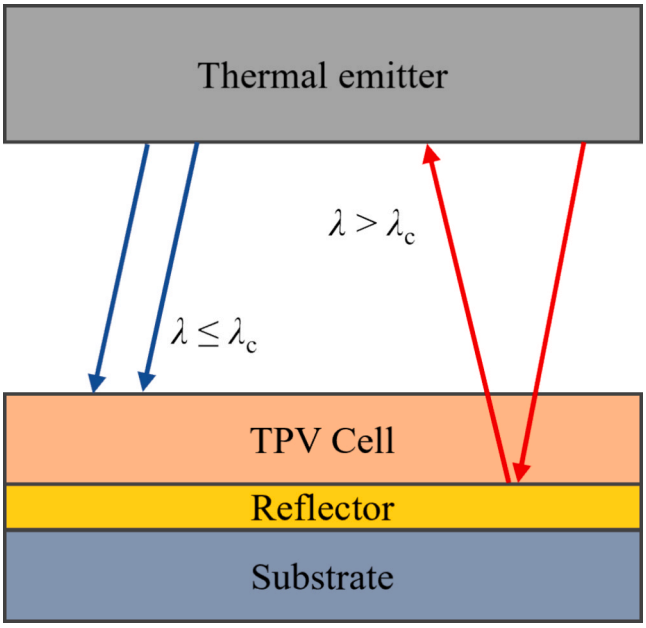

Fig. 3. The structure of TPV cell with BSR.

enclosed by high-performance thermal insulation to minimize heat loss. The system operation is governed by a mechanical actuation mechanism. To initiate power generation, the TPV cell is precisely engaged with the high-temperature emitter. During discharge, the PCM solidifies, releasing substantial latent heat at a nearly constant temperature. The emitter converts this heat into thermal radiation, which is then captured by the TPV cell and converted into electricity, ensuring a stable power output. To halt the process, the TPV cell is mechanically retracted from the emitter. The optimal design of this thermal cell system is explored through cost scaling analysis, focusing specifically on minimizing the CPE by optimizing parameters such as PCM thickness and other geometric dimensions [28]. Following the approach of Datas et al. [21], silicon (melting temperature: 1414 °C, density: 2.33 g/cm^3, latent heat: 1800 J/g, cost: 3.62 $/L) and FeSiB alloy (melting temperature: 1157 °C, density: 5.39 g/cm3, latent heat: 777 J/g, cost: 3.62 $/L) were selected as PCMs, as shown in Table 1. Alumina fiber mat and fumed silica board were used for thermal insulation. Through the design of reasonable structures, CPE values of 4.95 $/kWh (applicating FeSiB) and 6.27 $/kWh (applicating Si) were achieved.

2.2. Mathematical model of TPV system

This study applies a single diode numerical model of TPV cells with back surface reflectors (BSRs). The single diode model has been proven to be able to accurately predict the current–voltage (I-V) curve of the TPV system under given working conditions [33]. The BSRs are also widely used in various TPV systems to enhance efficiency by reflecting the sub-bandgap photons, which cannot be converted to electrical power [14,34,35]. Fig. 3 shows the concept of the BSRs.

The single diode equation is given by [33],

$$J = J_{ph} - J_0\left\{\exp\left[\frac{q}{nk_BT_c}(V + IR_s)\right] - 1\right\} - \frac{V + IR_s}{R_{sh}} \quad (1)$$

where J and V are current and voltage of TPV cell, respectively. The J_{ph} denotes the light generate current density, which can be approximated by the short circuit current density J_{sc} [36]. J_0 represents the reverse saturation current density, n is the diode ideality factor. The q, k_B and T_c denote the elementary charge, Boltzmann constant and cell temperature, respectively. R_s and R_{sh} are series resistance and shunt resistance, respectively.

The short circuit current density can be calculated by

$$J_{sc} = \int_{300nm}^{\lambda_c} \frac{\lambda}{hc} I_{BB} \bullet EQE_\lambda \bullet VF \bullet ed\lambda \quad (2)$$

where λ_c is cut-off wavelength, h and c denote Plank's constant and speed of light, respectively. I_{BB} represents the spectral radiant power density of TPV emitter which is assumed as a blackbody and VF is the view factor assumed as 1 in this system. λ_c is interpreted by

$$\lambda_c = \frac{hc}{E_g} \quad (3)$$

where E_g is the bandgap of the TPV cell.

EQE_λ is a function of external quantum efficiency of TPV cell in response to the wavelength. Spectral radiant power density is interpreted by Plank's law

$$I_{BB} = \varepsilon \frac{2\pi hc^2}{\lambda^5} \frac{1}{e^{hc/(\lambda k_B T_{emit})} - 1} \quad (4)$$

where T_{emit} is the emitter temperature, and ε denotes the emissivity of the emitter.

After drawing the I-V curve of the TPV cell under the given condition, the maximum power point (MPPT) can be traced, and thereby the maximum power density (P_M) can be calculated by

$$P_M = J_M V_M \quad (5)$$

where J_M and V_M are the current density and voltage at the MPPT.

The net thermal radiation from the emitter to TPV cell is the total incident radiation to the TPV minus the reflected radiation from the TPV cell, so the relationship between the net thermal radiation (Q_{net}) and the sub-bandgap reflectance r_{sub} is

$$Q_{net} = \int_{0.3\mu m}^{+\infty} I_{BB} \bullet VFd\lambda - \int_{\lambda_c}^{+\infty} r_{sub} \bullet I_{BB} \bullet VFd\lambda \quad (6)$$

Therefore, the output efficiency of TPV cell (η_{out}) is

Table 2
Three parameter configurations of TPV cells studied in this work.

Parameter	Description	Reference	Ideal	High-quality	Intermediate
n	Diode ideality factor (Degraded in intermediate case to reflect higher recombination current due to reduced manufacturing quality in large-scale production.)	1.098–1.171[33]	1.0	1.0	1.15
R_s ($\Omega\bullet cm^2$)	Series resistance	0.014–0.054 [33]	0	0.040	0.040
R_{sh} ($\Omega\bullet cm^2$)	Shunt resistance (Degraded to reflect lower shunt resistance caused by process defects like microcracks, scratches common in large-scale production.)	92–1162 [33]	10^4	10^3	10^2
J_0 (A/cm^2)	Reverse saturation current density (Degraded in intermediate case to reflect higher recombination current due to reduced manufacturing quality in large-scale production.)	$1.5 \times 10^5 \exp(-qE_g/k_B T_c)$ (Model III in ref [[38])	$1 \times$ Model III	$3 \times$ Model III	$3 \times 10^3 \times$ Model III
EQE	External Quantum Efficiency	–	0.9	0.9	0.9
r_{sub}	Sub-bandgap reflectance	0.95 [34], 0.98 [35]	1	0.95	0.95

$$\eta_{out} = \frac{P_M}{Q_{net}} \times 100\% \tag{7}$$

In this study, three groups of typical single diode parameters are analyzed. These groups of parameters are called ideal, high-quality, and intermediate TPV cells, which correspond to different levels of manufacturing technologies. The high-quality configuration corresponds to the TPV cell well made in the laboratory, whereas the intermediate configuration represents the cells made from a large-scale production process. The low R_{sh} is usually caused by many types of process failures, such as microcracks, scratches, or improper wafer dicing [37]. The stochastic characteristic of these defects makes them hard to control in large-scale production, so the R_{sh} reflects the lower bound of production quality. The J_0 is a sum of different recombination current densities in different parts of the TPV cell, which can reflect the overall manufacturing quality. Hence, the R_{sh} and J_0 (and its related n) are chosen to be degraded in the intermediate configuration. The influences of other parameters on the economic results are studied in the sensitivity study section. The parameters configurations are listed in the Table 2.

2.3. Techno-economic metrics

The economic viability of an energy storage system is commonly evaluated using LCOS, which represents the comprehensive lifetime cost per unit of discharged energy ($/kWh). As an integrative metric, the LCOS is fundamentally determined by key technical and economic parameters. Furthermore, it is crucial to explore how individual technical metrics influence a system's suitability for various market applications. The main techno-economic metrics are detailed below.

(1) Energy Density (kWh/m^3): This metric represents the energy capacity stored per unit volume of the entire system. A higher energy density corresponds to a smaller physical footprint, which in turn yields substantial cost savings in land acquisition, civil works, and installation, especially for space-constrained applications. (2) Roundtrip efficiency (η_{rt}), which is computed by the electricity input efficiency and output efficiency ($\eta_{rt} = \eta_{in}\bullet\eta_{out}$). A lower efficiency signifies greater energy losses, meaning more input electricity must be purchased to deliver the required output. Roundtrip efficiency is a primary driver of the LCOS, as the cumulative cost of these energy losses over the system's operational lifetime directly increases the overall cost. (3) Daily self-discharge rate (%/day): This parameter quantifies the rate at which a system's stored energy dissipates due to internal processes, such as heat loss in thermal storage, during idle periods. For long-duration storage applications, a high self-discharge rate is particularly detrimental. It necessitates more frequent recharging cycles to maintain a state of readiness, thereby increasing operational expenditures and growing the overall LCOS. (4) Response time: This metric defines the time required for a storage system to ramp from an idle or charging state to its target power output following a dispatch signal. This time is a critical factor in determining its revenue streams. Specifically, faster response capabilities enable participation in lucrative service markets. (5) Service life (years): This parameter refers to the operational duration over which a system can perform according to its specified technical requirements. Service life is a foundational component in LCOS calculation. A longer operational lifetime allows the initial capital expenditures (CPE and CPP) to be amortized over a greater cumulative energy output, thereby lowering the LCOS. (6) Cost per energy capacity (CPE, $/kWh): This metric represents the capital cost of components dedicated to storing energy, including the storage medium, containment, and thermal insulation. As a foundational component of LCOS, CPE is particularly impactful for long-duration storage systems where energy capacity is the dominant cost driver. Reducing CPE is a paramount objective for realizing economically viable, large-scale energy storage. (7) Cost per power (CPP, $/kW): This metric includes the capital cost of the power conversion system and other components essential for charging and discharging. As a key component of the LCOS, CPP is the dominant cost driver for high-power, short-duration applications. (8) Levelized cost of storage (LCOS, $/kWh): As the principal metric for assessing the economic feasibility of an energy storage system, the LCOS provides a comprehensive figure of merit. It integrates the most of related techno-economic parameters, including CPE, CPP, roundtrip efficiency, self-discharge rate and the system's service life. The LCOS is calculated as the ratio of the total life-cycle cost to the total lifetime discharged energy.

While recent studies have proposed metrics for the economic analysis of energy storage [19,21], their formulations have limitations. For instance, the LCOS model in literature [21] omits operation and maintenance (O&M) costs. Similarly, the LCOE model in literature [19] does not account for the cost of storage equipment, limiting its applicability to EES. To address these limitations, this work introduces a comprehensive LCOS formulation that incorporates O&M costs, which is suitable for TPVES.

$$\mathrm{LCOS} = \frac{p_e}{\eta_{rt}} + \frac{1}{N_{cycle}}\left(\frac{\mathrm{CPP}^*_{in}}{\eta_{rt} t_c} + \frac{\mathrm{CPE}^*}{\eta_{out}} + \frac{\mathrm{CPP}^*_{out}}{t_d} + \frac{CPOM}{t_d}\right) \tag{8}$$

where p_e is the price of input energy, η_{rt} denotes round-trip efficiency of energy storage system, N_{cycle} represents the charging and discharging cycles in 1 year, CPP^*_{in} and CPP^*_{out} denotes the annualized cost per power and cost per energy capacities respectively, t_c and t_d denotes charging and discharging time respectively, η_{out} denotes the output efficiency of the system and $CPOM$ denotes the cost of operation and maintenance of system in 1 year. The round-trip efficiency of system can be calculated by

$$\eta_{rt} = \eta_{in}\bullet\eta_{out} \tag{9}$$

where η_{in} denotes charging efficiency. N_{cycle} can be computed by

$$N_{cycle} = 8760/(t_c + t_d)$$

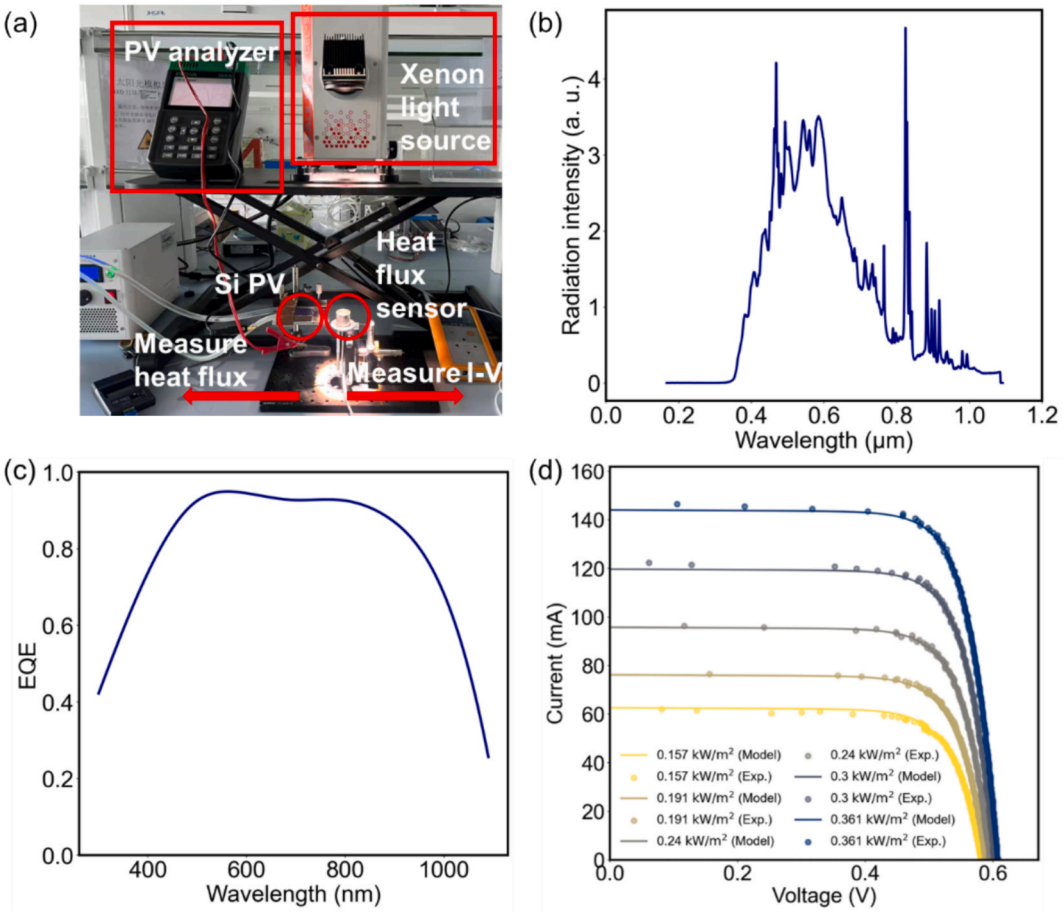

Fig. 4. The experimental validation. (a) The experimental setup for validation. (b) The radiation intensity spectrum of the commercial Xenon light . Source. (c) EQE of the crystalline silicon cell tested in this validation, details about EQE data can be found in the Supplementary Information section. (d) Comparison results of measured I-V data (semi-transparent dots) and I-V curves calculated by this work's single diode computer program (lines)

Table 3
The extracted single diode parameters from the first 2 I-V curves.

Parameter	Extracted from first 2 I-V curves
n	1.44
R_s (Ω•cm^2)	0.157
R_{sh} (Ω•cm^2)	7272
J_0 (A/cm^2)	1.16 × 10^{-9}

CPX* is interpreted by annualized law

$$\mathrm{CPX}^* = CPX \cdot \frac{r(1+r)^n}{(1+r)^n - 1} \tag{10}$$

where r denotes discount rate and n represents the service life of the system. The cost of per output power (CPP $_{out}$) can be calculate by

$$CPP_{out} = \frac{C_{cell}}{p_m} \tag{11}$$

where C_{cell} denotes the cost of TPV cell and p_m denotes the maximum power density of TPV generator.

2.4. Experimental validation

To validate the accuracy of the power generation model and corresponding single diode calculation program, an experimental test was conducted. 5 I-V curves are measured under the 5 different incident radiation densities. The 2 I-V curves correspond to the first and second minimum radiation densities are utilized to extract the n, R_s, R_{sh} and J_0 parameters of the very cell tested in this experiment. The method of the parameter extraction is Trust Region Reflective (TRR) algorithm, which's validity of extracting the single diode model from I to V curve has been proven in literature [39]. 3 more I-V curves are predicted at 3 higher radiation densities via model extrapolation with TRR extracted parameters, then they are compared with the 3 corresponding experimental measured I-V curves.

Fig. 4(a) shows the experiment setup. In order to ensure the precision of incident radiation spectrum, the heat source in this experiment is a standard commercial Xenon light source with an optical filter (Beijing China Education Au-light Co., Ltd.), and the incident spectrum is shown in Fig. 4(b). A 3 × 3 cm crystalline silicon photovoltaic cell was bonded to a copper water-cooling plate using an electrically insulating, high-thermal-conductivity silicone grease, with a thermocouple attached to the back of the cell to measure its temperature in real time. Unencapsulated silicon PV cell without backsheet or potting was utilized to enhance the cooling and the accuracy of temperature measurement, hence the parameters of this test cell might slightly beneath the common commercial photovoltaics' standards. The laboratory chiller pumps and chills the cooling water for the cell, the temperature of the cooling water is controlled around 23℃. In this verification experiment, the crystalline silicon cell was connected to a PV analyzer using gold-plated Kelvin clips based on the four-wire measurement method commonly employed for solar cell characterization. To get the relatively stable incident radiation, the measurements are conducted 25–30 min after turning on the Xenon lamp, and the heat flux sensor maintains on the same height with the silicon cell.

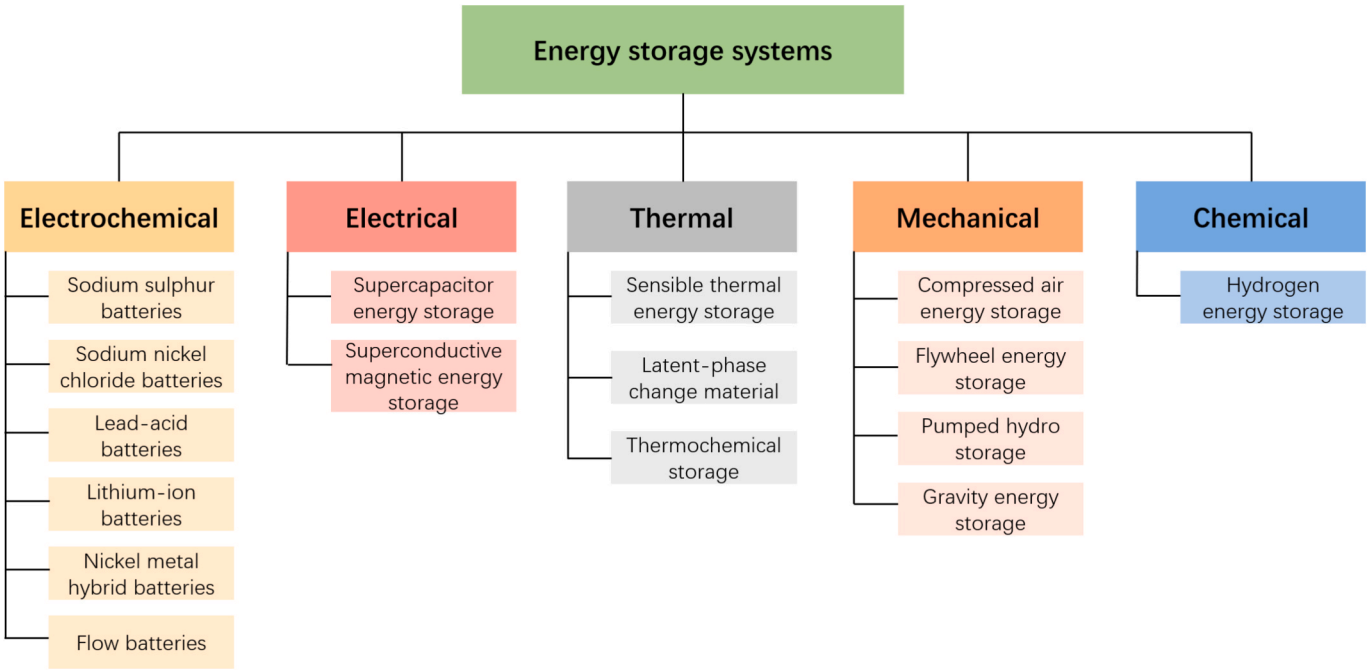

Fig. 5. Classification of energy storage systems.

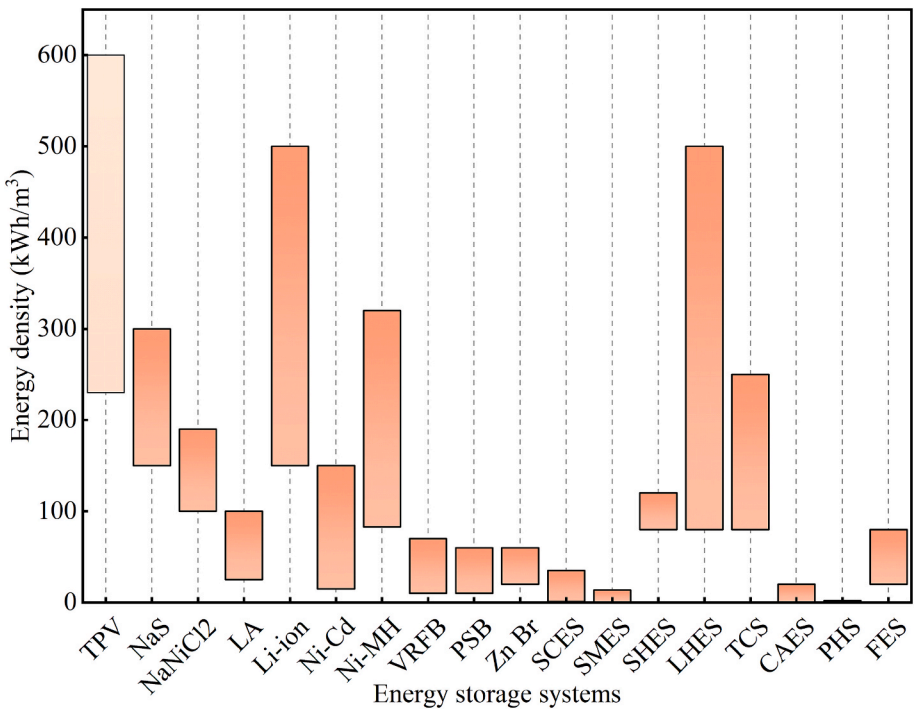

Fig. 6. Energy density of TPV and selected energy storage systems. The detailed data are collected from: TPV[21], NaS [40,41,42,43], $NaNiCl_2$ [40,44], LA [40,44], Li-ion [40,44,45], Ni-Cd [40,46], Ni-MH [40,47,48], VRFB [49,50], PSB [51,52], Zn Br [40,53,54], SCES [55,56], SMES [44,55], SHES[52], LHES [40,52], TCS [40], CAES [40,55,57], PHS [42,52,55,57], FES[40].

There are some assumptions in this experimental validation. The cell temperature has been measured at the several points across the cell area, and the temperature difference between points are below 0.5℃, hence in the calculation, the temperature of the cell is assumed to be uniform. The extracted parameters from the first 2 I-V curves are listed in Table 3. In the calculation, the EQE spectrum is a 8th-degree polynomial curve fitted from the original measured EQE data points. The detailed information about the measurement and data processing of the EQE is provided in the supplemental information section. The EQE spectrum of the silicon photovoltaic cell in this study is shown in Fig. 4(c).

During the experiment, the cell temperature varied from 25.6 to 25.9℃, so the influence of cell temperature can be ignored, and in the calculation, the cell temperature is fixed to 26℃. As shown in Fig. 4(d), the calculated I-V curves match well with the experimentally measured data. The overall RMSE of current between the calculated and measured data is 3.3 mA, and the RMSE in the extrapolation area (the 0.24, 0.3 and

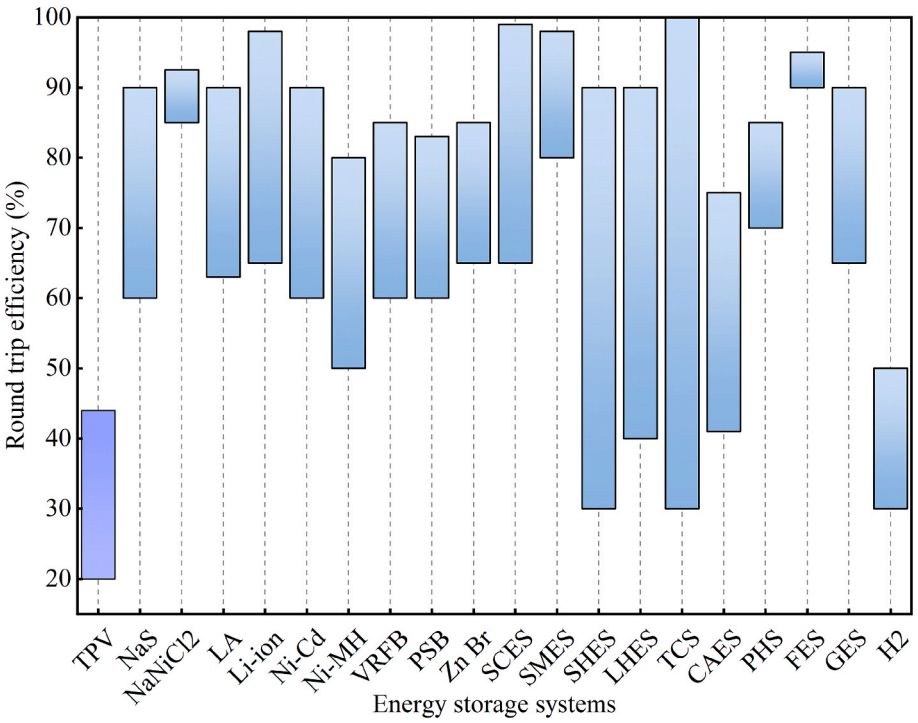

Fig. 7. Round trip efficiency of TPV and selected energy storage systems. Data for comparison are from: TPV [12,14,58], NaS [40,44,51,59,60], $NaNiCl_2$ [51,61], LA [42,44,50,52,59,62], Li-ion [44,50,51,59,60], Ni-Cd [40,51,59], Ni-MH [40,62], VRFB [40,51,59,63], PSB [40,44], Zn Br [40,44,51,64], SCES [40,44,51], SMES [44] [46], SHES [59,65,66], LHES [40,59,65,67], TCS [65,67,68], CAES [59], PHS [59], FES [59], GES [59], Hydrogen [59].

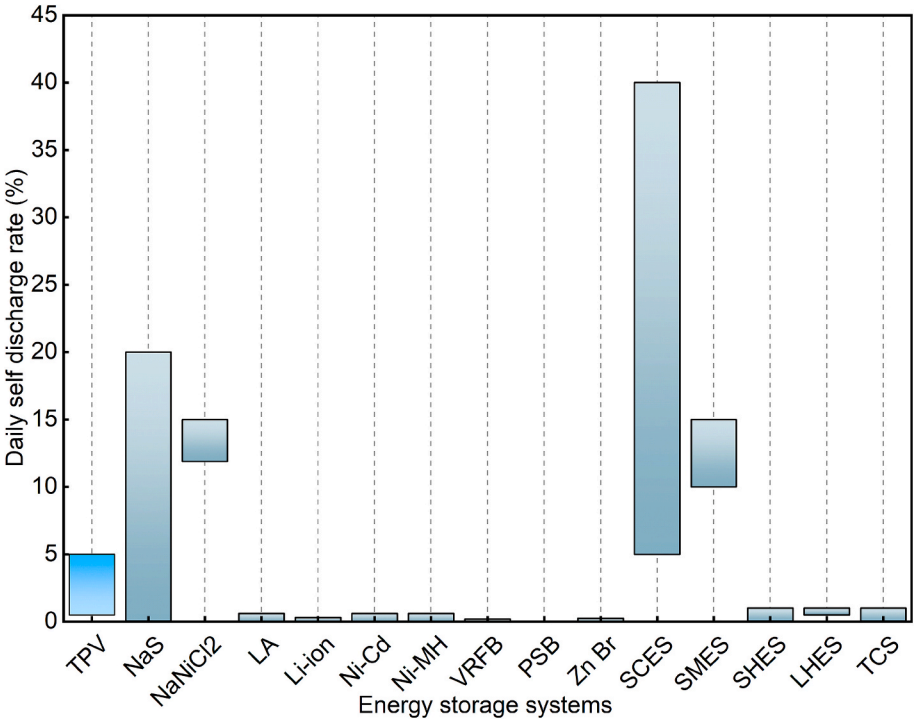

Fig. 8. Daily self-discharge rate of TPV and selected energy storage systems. Data for comparison are from: TPV[21], NaS[51,52], $NaNiCl_2$[40,51], LA[40,51,69], Li-ion[11,40,70], Ni-Cd[44,51,52,71], Ni-MH[71,72], VRFB[44,51,52], PSB[51,52], Zn Br[51,52], SCES[50,51,52], SMES[51,52], SHES[52,66], LHES[52], TCS[66].

0.361 kW/m^2 radiation density) is 2.9 mA. While these RMSE values are sufficiently low to demonstrate a strong fit, the minor discrepancies observed can be attributed to several potential factors. Primarily, the single-diode model is an idealized representation and may not perfectly capture all non-linear recombination mechanisms within the physical cell. Furthermore, the model parameters were extracted at lower irradiance levels; any slight dependence of these parameters such as series and shunt resistance on irradiance could introduce small errors when extrapolating to higher radiation densities. Finally, minor experimental uncertainties, such as the precision limits of the heat flux sensor or slight

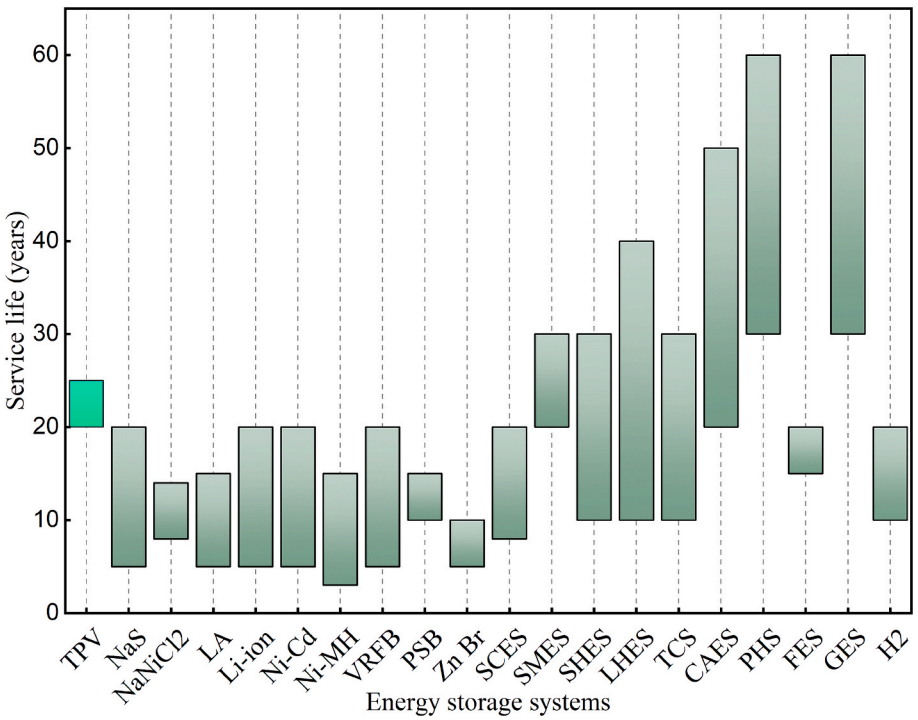

Fig. 9. Service life of TPV and selected energy storage systems. Data for comparison are from: TPV[19,21], NaS[40,44,51,59], $NaNiCl_2$[40,51], LA[44,52,59], Li-ion [44,47,52,59], Ni-Cd[51,52,59], Ni-MH[40,47], VRFB[44,51,59], PSB[44,51], Zn Br[44,51], SCES[44,51,52], SMES[40,44], SHES[40,52], LHES[52,59,73,59], TCS [40,73], CAES[59], PHS[59], FES[59], GES[59], Hydrogen[59].

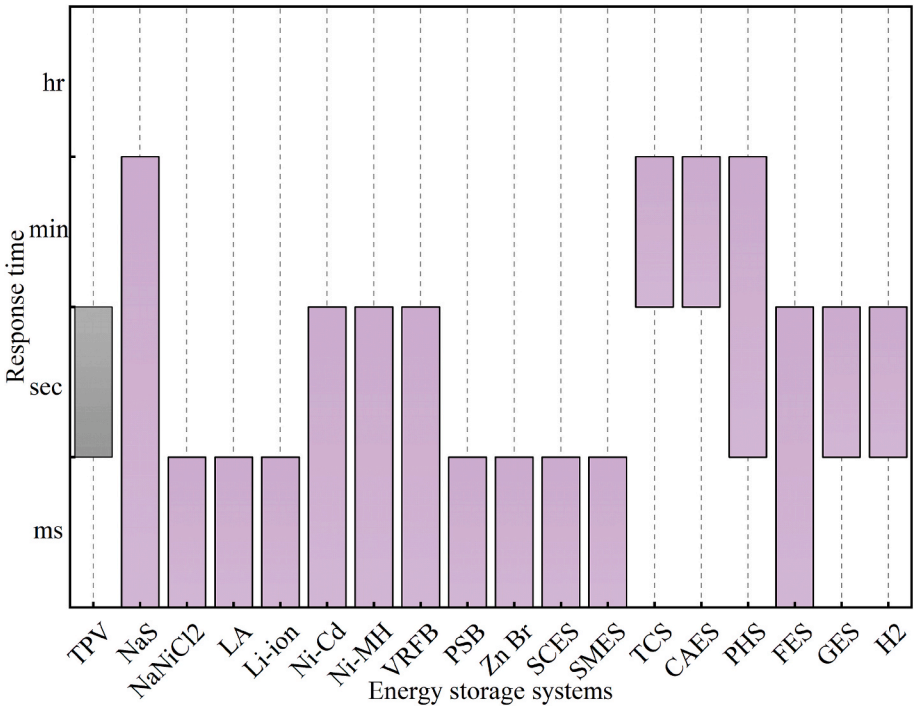

Fig. 10. Response time of TPV and selected energy storage systems. Data for comparison are from: NaS[46], $NaNiCl_2$[59], LA[74], Li-ion[59], Ni-Cd[46], Ni-MH [75], VRFB[46], PSB[76], Zn Br[77], SCES[46], SMES[46], TCS[74], CAES[74,40], PHS [40], FES[46], GES[59], Hydrogen[59].

fluctuations in the Xenon lamp spectrum, may also contribute to the deviation. Nevertheless, the close agreement between the calculated and measured data, as evidenced by the low RMSE values, confirms the validity of the single diode model and calculation program.

3. Results and discussions

To evaluate the development prospects of TPVES, this study compiles the key techno-economic metrics for five major categories of current mainstream energy storage systems, as categorized in Fig. 5: Electrochemical storage encompasses Lithium-ion (Li-ion), Lead-acid (LA),

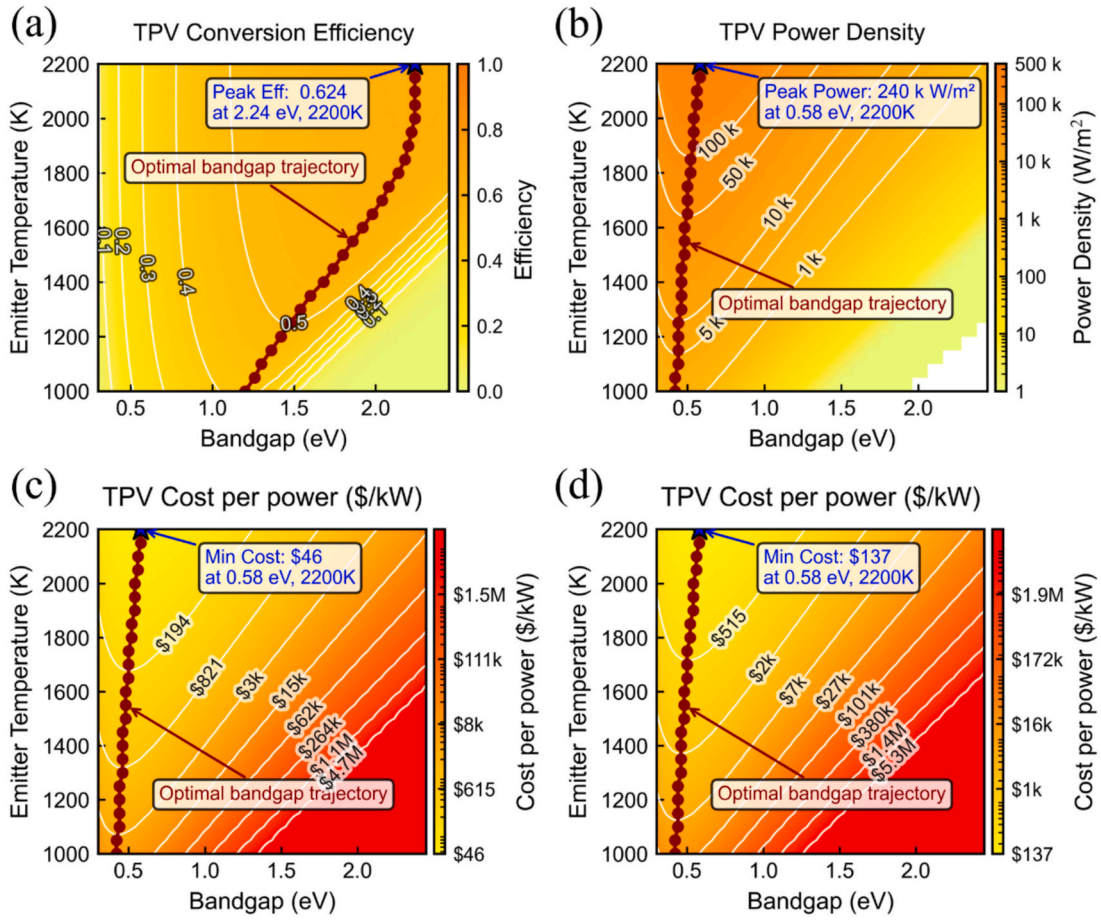

Fig. 11. Conversion efficiency, power density and CPP of ideal TPV generator under varying bandgaps and emitter temperatures. (a) TPV conversion efficiency. (b) TPV power density. (c) CPP of TPV cell cost at \$1.1/cm^2; (d) CPP of TPV cell cost at \$3.3/cm^2. Simulations assume a blackbody emitter, TPV cell temperature fixed at 298 K, single-junction cells, 90 % quantum efficiency, unity view factor, and the TPV cell cost range of 1.1–3.3\$/cm^2. [21,87]. The ideal TPV parameters assume diode ideality factor of 1, $R_s = 0$ Ω·cm^2, $R_{sh} = 10^4$ Ω·cm^2, $J_0 = 1 \times$ model, 100 % reflectance for sub-bandgap photons. In all subplots, the solid dark red line represents the optimal bandgap trajectory that best value for a given temperature. The blue triangles mark the optimal values for each metric and the corresponding operating conditions.

Sodium-sulfur (NaS), Sodium-nickel chloride ($NaNiCl_2$), Nickel-metal hydride (Ni-MH), Nickel-cadmium (Ni-Cd), Polysulfide-bromine flow (PSB), Vanadium redox flow (VRFB), and Zinc-bromine flow (ZnBr) batteries; Electrical storage includes Superconducting magnetic energy storage (SMES) and Supercapacitor energy storage(SCES) systems; Thermal storage comprises Sensible heat energy storage (SHES), Latent heat energy storage (LHES), and Thermochemical storage(TCS) systems; Mechanical storage involves Compressed air (CAES), Flywheel (FES), Pumped-hydro (PHS), and Gravity (GES) energy storage; and Chemical storage features Hydrogen storage system. Furthermore, this work proposes a mathematical model to calculate specific economic parameters for the TPVES and reviews established technical analyses recent journals.

Detailed graphical analysis and comparative characteristics of these technologies are presented in Sections 3.1 and 3.2, facilitating the selection of the most suitable storage technology for specific applications and summarizing their respective advantages and disadvantages.

3.1. Technical analysis

The key technical performance parameters of TPVES and selected energy storage systems are summarized in Supplementary Table 1. The detailed data is collected from previous peer-reviewed journals, websites and books. Considering the reported data for EES can vary significantly across literature sources—influenced by factors such as scale, geographical location, and technological maturity—the following figures are presented to encompass the full range of collected values. This approach ensures a comprehensive and objective comparison by illustrating the data spread for each technology rather than relying on single point-estimates. Comparative graphical assessments are further provided in Figs. 6–10.

Fig. 6 illustrates a comparison of the volumetric energy density (kWh/m^3) of the TPVES against several other mainstream storage technologies. As a key metric, energy density represents the amount of energy that can be stored per unit volume of the entire system. A higher energy density corresponds to a smaller physical footprint, which in turn yields substantial cost savings in land acquisition and installation, especially for space-constrained applications.

As is evident from the chart, the TPVES exhibits a remarkable energy density, ranging from 230 to 600 kWh/m^3, which is superior to the other compared technologies. Specifically, the energy density of TPV is not only significantly higher than conventional systems such as LA, Ni-Cd, and various flow batteries (e.g., VRFB), but it also surpasses that of the widely adopted Li-ion batteries. This high energy density indicates that a greater amount of energy can be stored within a smaller physical volume, consequently positioning TPV technology as a particularly promising solution for energy storage in space-constrained environments, such as densely populated urban areas.

As depicted in Fig. 7, a comparative analysis of round-trip efficiency highlights a key challenge for TPVES relative to other ESS. Round-trip

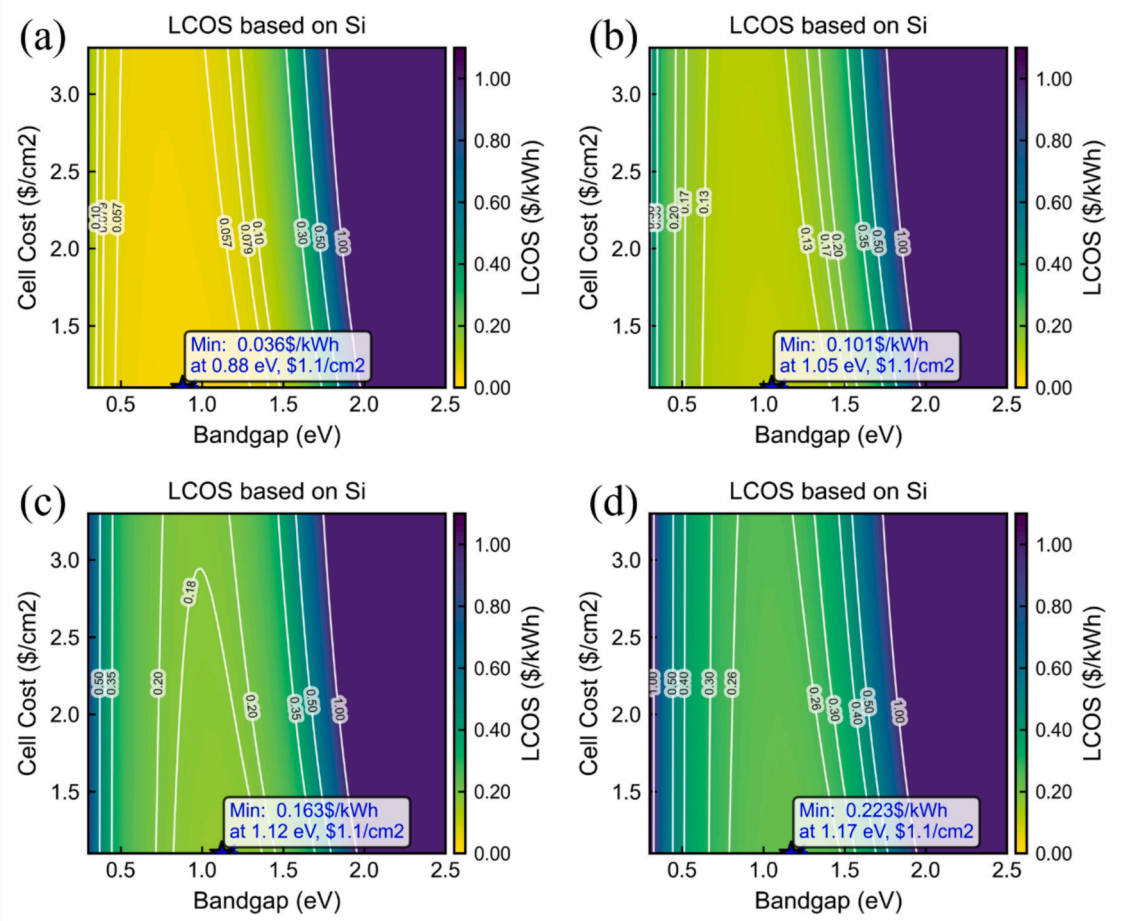

Fig. 12. LCOS of the ideal TPVES system based on Si under varying electricity input prices. (a) electricity of 0.01$/kWh, (b) electricity of 0.04$/kWh, (c) electricity of 0.07$/kWh, (d) electricity of 0.10$/kWh. Simulations assume the system capacity of 100 MWh, reflector cost = 1.03$/m^2[88], discount rate of 7 %, system lifetime of 25 years, charging time of 5 h and discharging time of 10 h. [20,21,89]. Other parameters consistent with Fig. 11.

efficiency, a critical metric defined as the product of the input and output efficiencies, directly governs the economic feasibility of a storage system. It quantifies the energy losses over a complete charge–discharge cycle. A lower efficiency signifies greater energy losses, which leads to higher operational expenditures, as more input electricity must be purchased to deliver the required output, and ultimately contributes to a higher LCOS.

A significant drawback of TPVES is its comparatively low round-trip efficiency. This is starkly illustrated when compared with mature electrochemical technologies. For example, Li-ion batteries can achieve efficiencies as high as 98 %, while NaS and LA batteries both operate at approximately 90 %. Even when compared to large-scale physical storage systems such as PHS and CAES, TPVES's performance is at a disadvantage. The maximum 44 % efficiency of the TPVES presented here signifies substantial energy losses. Consequently, the application of TPVES has been largely confined to scenarios where the economic penalty of low efficiency is mitigated by low-cost input energy, such as wind and solar energy. Despite this clear limitation, the technology is on a promising trajectory. Recent breakthroughs have enabled TPV efficiency to reach 44 %, which is a notable achievement compared to about 20 % in 10 years ago. This rapid progress suggests that as the technology matures, the efficiency gap will continue to narrow, unlocking a much broader range of future applications for TPVES.

Fig. 8 demonstrates the daily self-discharge rate of the TPVES in comparison to other technologies. This parameter quantifies the rate at which a system's stored energy dissipates due to internal processes, such as heat loss, during idle periods. For long-duration storage applications, a high self-discharge rate is particularly detrimental, as it necessitates more frequent recharging cycles to maintain a state of readiness, thereby increasing operational expenditures and the overall LCOS.

As shown in the figure, TPVES presents a moderate self-discharge rate of approximately 2–5 %/day. While this is slightly higher than near-zero-loss electrochemical systems like Li-ion, LA, and various flow batteries, which have rates of < 1 %/day, it is substantially lower than systems with high self-discharge, such as high-temperature NaS batteries and SCES. This self-discharge in TPV systems is primarily attributed to thermal losses, a factor that can be effectively mitigated by improving thermal insulation. Considering the relatively low CPE of TPVES, this manageable thermal loss does not significantly impact its overall economic feasibility. Furthermore, for typical storage durations of less than one day, the cumulative energy loss is often negligible.

Fig. 9 illustrates the service life of the TPVES in comparison to other EES. Service life refers to the operational duration over which a system can perform according to its specified technical requirements and is a foundational component in the calculation of the LCOS. A longer operational lifetime allows the initial capital expenditures to be amortized over a greater cumulative energy output, thereby lowering the LCOS.

As shown in the figure, TPVES demonstrates a distinct durability advantage over all surveyed electrochemical and chemical storage technologies. Specifically, its lifespan surpasses that of most electrochemical storage technologies, such as Li-ion batteries and lead-acid batteries, as well as FES. The lifespan of TPVES is comparable to that of most electrical (e.g., SMES) and thermal storage systems (e.g., LHES, TCS). Although its service life is shorter than large-scale mechanical

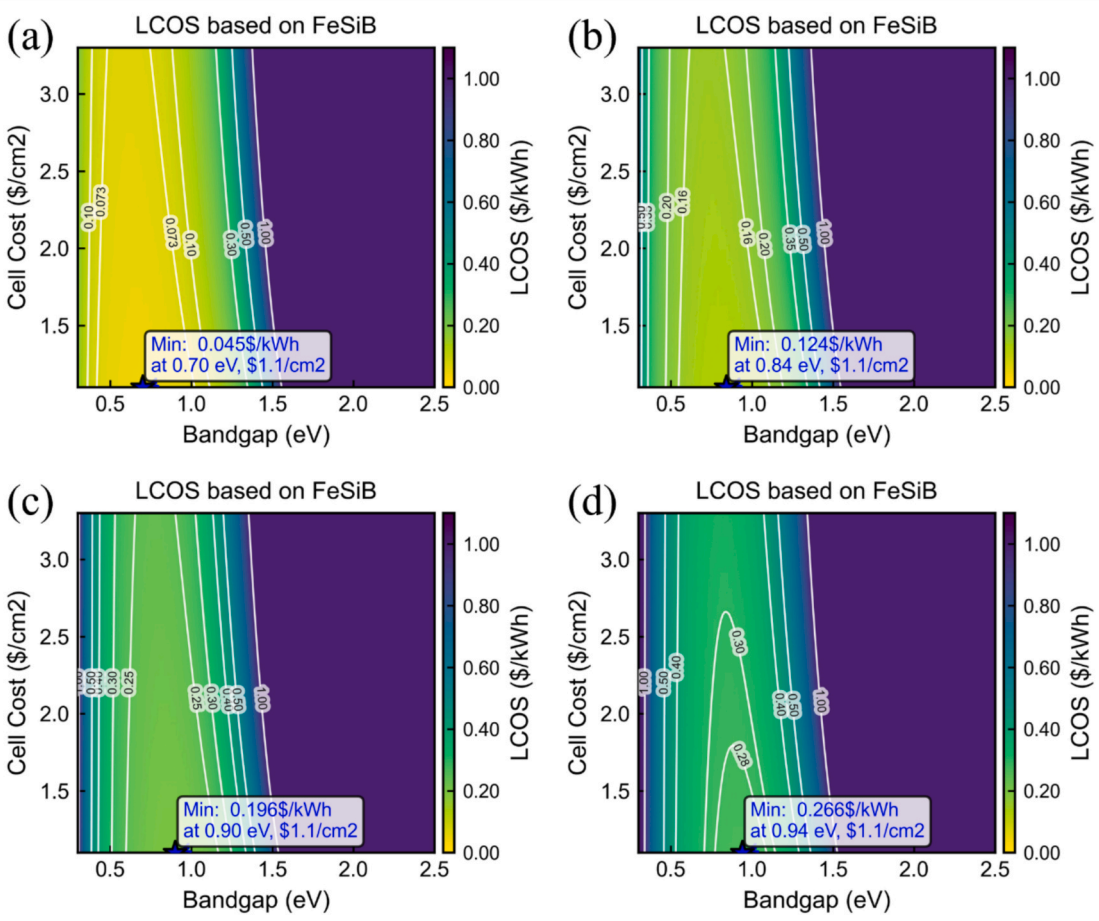

Fig.13. LCOS of the ideal TPVES system based on FeSiB under varying electricity input prices. (a) electricity of 0.01$/kWh, (b) electricity of 0.04$/kWh, (c) electricity of 0.07$/kWh, (d) electricity of 0.10$/kWh. Other parameters consistent with Fig. 12.

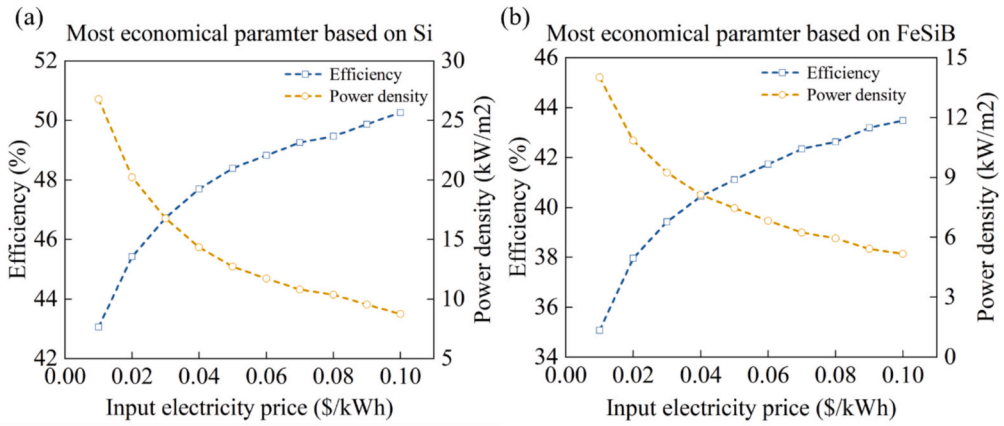

Fig.14. The most economical parameter of the ideal TPVES under varying electricity input prices. (a) the energy storage material uses Si, (b) the energy storage material uses FeSiB. Other parameters consistent with Fig. 12.

storage systems with extremely long lifespans like PHS, this competitive service life is a key metric for achieving a favorable LCOS, confirming the potential of TPV technology and establishing its feasibility for long-term deployment.

Fig. 10 compares the response time of the TPVES with other EES. Response time is the metric defining the time required for a storage system to ramp from an idle or charging state to its target power output following a dispatch signal. This is a critical factor in determining its potential revenue streams, as faster response capabilities enable participation in lucrative ancillary service market.

As demonstrated in the figure, TPVES exhibits a response time on the order of seconds, positioning it moderately among comparable technologies. Specifically, while it is slower than electrochemical and electrical storage systems like Li-ion batteries, LA, and SMES, which can respond on a millisecond scale, TPVES is significantly faster than technologies requiring minutes to hours to ramp up, such as CAES and TCS. This second-scale response time, which primarily reflects the mechanical translation of the TPV generator assembly, satisfies the operational

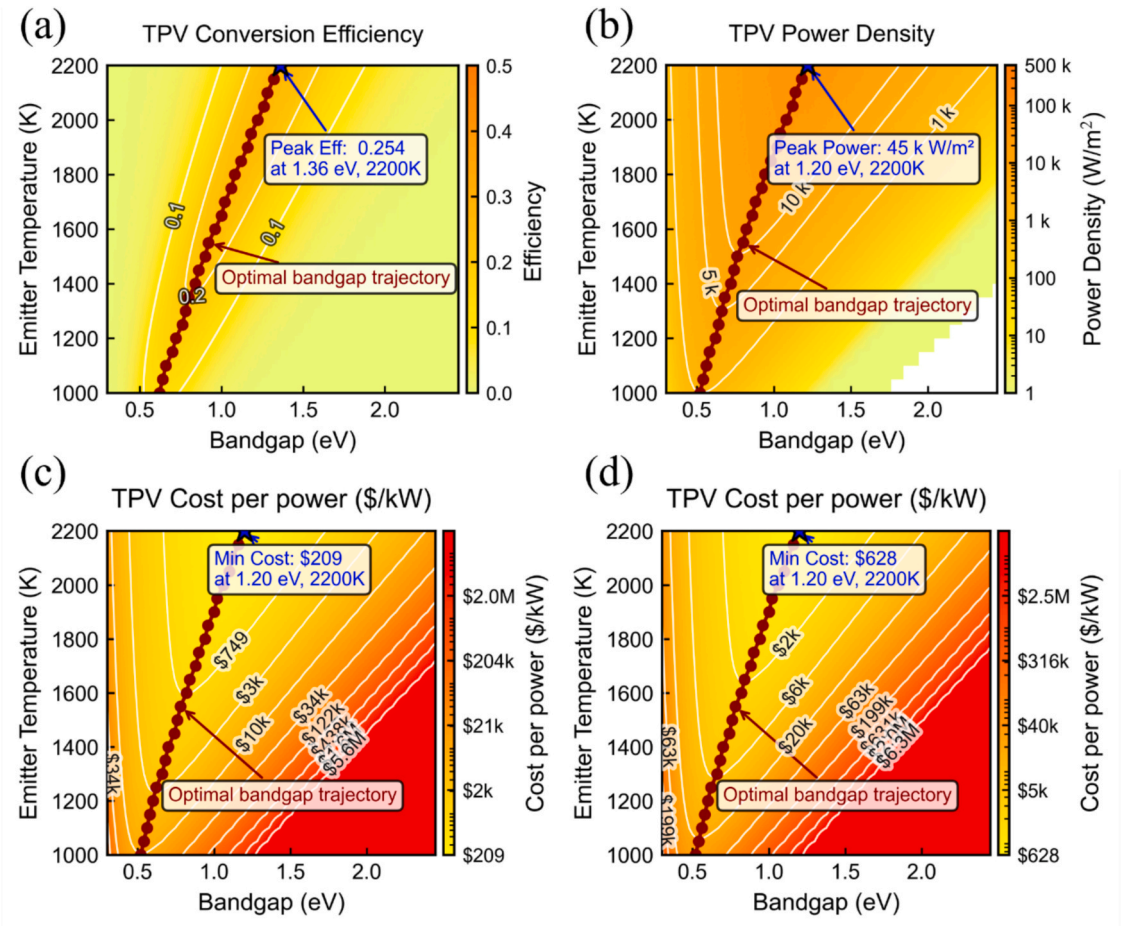

Fig.15. Conversion efficiency, power density and CPP of high quality TPV generator under varying bandgaps and emitter temperatures. (a) TPV conversion efficiency. (b) TPV power density. (c) CPP of TPV cell cost at $1.1/cm^2; (d) CPP of TPV cell cost at $3.3/cm^2. The high quality TPV parameters assume diode ideality factor of 1, $R_s = 0.04\ \Omega{\cdot}cm^2$, $R_{sh} = 10^3\ \Omega{\cdot}cm^2$, $J_0 = 3 \times$ model, 95 % reflectance for sub-bandgap photons. Other parameters consistent with Fig. 11.

requirements for many grid integration applications.

Collectively, the moderate response performance of TPVES, combined with its other key advantages like high energy density and long service life, positions it as a transformative and viable solution for space-constrained applications.

3.2. Economic analysis

TPVES are primarily composed by heating system, thermal storage system and TPV generator. This work utilizes advanced and low-cost technologies for heating and thermal storage components: ohmic heating and PCMs, which have been applied in literature [21]. The cost per power input (CPP $_{in}$) for resistive heaters exhibits significant temperature dependence [78]. Metallic alloy heating elements operating at maximum temperatures ≈1200 °C demonstrate CPP $_{in}$ values approximately 3.3 $/kW, while silicon carbide (SiC) heaters capable of higher operating temperatures (>1600 °C) show substantially higher CPP $_{in}$ ≈22 $/kW [21,79]. The selected PCMs are FeSiB (melting point: 1430 K, CPE: 4.95$/kWh) and Si (melting point: 1687 K, CPE: 6.27$/kWh) [21].

TPV generator first developed by Henry H. Kolm at MIT in 1956 [80], historically suffered from low conversion efficiency. This limitation confined its applications primarily to specialized military markets until recent decades [81]. Subsequent research revealed that integrating back-surface reflectors effectively enhances system efficiency [82], which has achieved at 44 % [14] recently. The technological advancement reignites significant research interest in TPV systems. Accordingly, this study establishes computational models for three distinct TPV generator configurations combined with heating and thermal storage system to evaluate the key economic metrics of the TPVES. For this economic analysis, the complex process of PCM operation within its latent heat range is simplified by assuming a constant temperature, thereby omitting the losses due to temperature changes during charging and discharging.

3.2.1. Ideal TPV generator with storage system

The conversion efficiency and power density of TPV generator are primarily determined by the bandgap energy of TPV cell materials and emitter operating temperatures. To optimize these parameters in ideal TPV generator, this study establishes a computational model identifying optimal bandgap-temperature pairings. Fig. 11 presents the key performance and economic metrics of a TPV system across varying emitter temperature (1000 K to 2200 K) and cell bandgap (0.3 eV to 2.4 eV). This analysis aims to reveal the critical trade-offs in system design and identify the optimal operating points for different optimization goals.

Fig. 11a shows the theoretical conversion efficiency of the TPV generator. It is evident that efficiency increases significantly with emitter temperature. For given temperature, there exists an optimal bandgap that maximizes efficiency, which clearly shows that the optimal bandgap shifts to higher values as the emitter temperature rises. Within the studied parameter range, a peak efficiency of 62.4 % is achieved at an emitter temperature of 2200 K and a cell bandgap of 2.24 eV. Fig. 11b presents the output power density of the TPV system. The system achieves significantly higher power densities than photovoltaics (PV), reaching 240 kW/m^2 at 2200 K, which is over three orders of

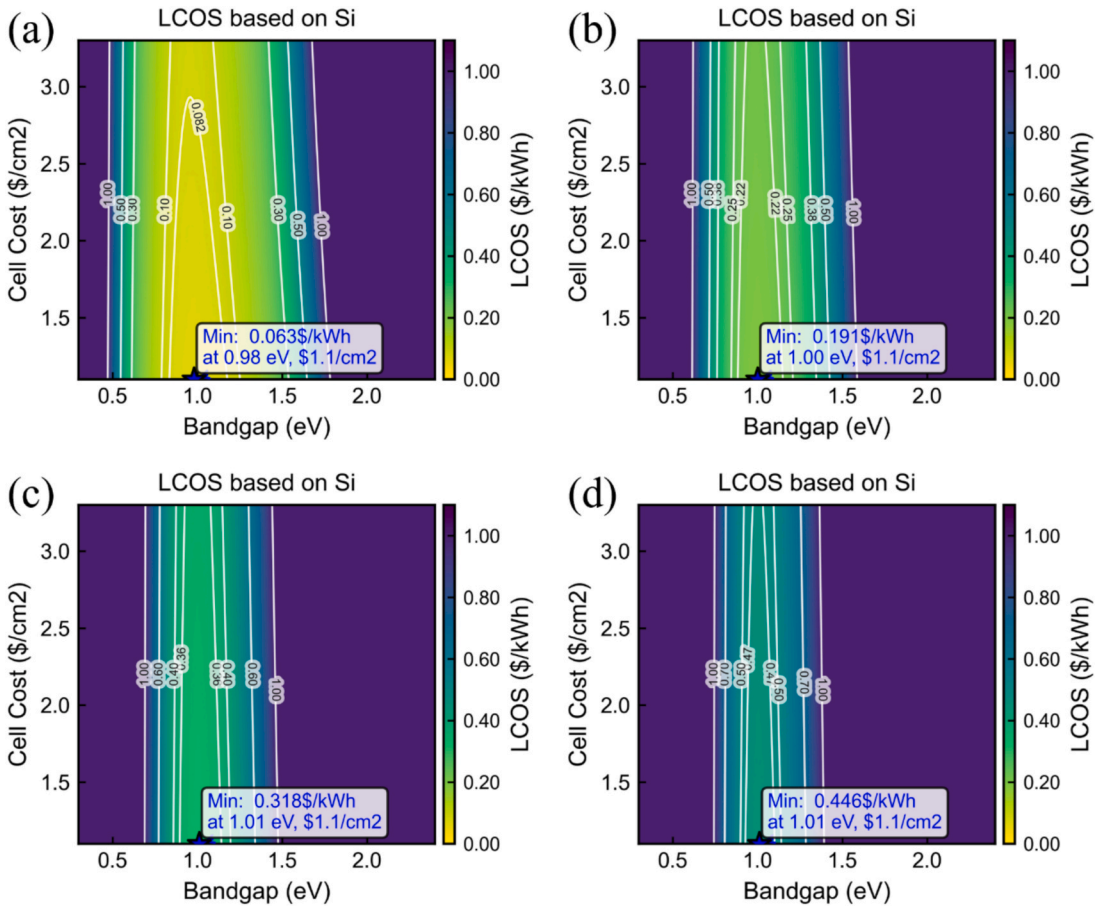

Fig.16. LCOS of the high quality TPVES system based on Si under varying electricity input prices. (a) electricity of 0.01$/kWh, (b) electricity of 0.04$/kWh, (c) electricity of 0.07$/kWh, (d) electricity of 0.10$/kWh. Simulations assume the system capacity of 100 MWh, reflector cost = 1.03$/m^2[88], discount rate of 7 %, system lifetime of 25 years, charging time of 5 h and discharging time of 10 h. [20,21,89]. Other parameters consistent with Fig. 15.

magnitude greater than the typical PV value of 273 W/m^2 [83,84]. This demonstrates TPV can release large amounts of energy within short time. Similar to efficiency, the power density increases dramatically with emitter temperature, consistent with the principles of thermal radiation described by the Stefan-Boltzmann law [85]. However, in contrast to efficiency, the peak power density occurs at a much lower bandgap. The maximum power density reaches 240 kW/m^2 under the conditions of 2200 K and 0.58 eV bandgap. Notably, the bandgap for maximum power (0.58 eV) is far from the bandgap for maximum efficiency (2.24 eV). This reveals a fundamental trade-off between optimizing for efficiency and optimizing for power density in TPV system design. Fig. 11c-d analyze the system's CPP, which is determined by power density and cell cost per unit area, exhibiting a corresponding relationship with power density at fixed cell prices. The common trend in both plots is that the CPP decreases with increasing emitter temperature and decreasing bandgap. This is because higher temperatures and lower bandgaps yield higher power densities, as shown in Fig. 11b. Consequently, the TPV system can achieve a CPP in the range of 46–137 $/kW, a value substantially more competitive than other energy storage technologies. This favorable economic performance is attained because the system's high power density effectively offsets the expensive cell costs, at 1.1–3.3$/cm^2 [21,86].

The results reveal a core trade-off in TPV system design: while maximizing conversion efficiency necessitates wide-bandgap cell materials, maximizing power density and minimizing CPP require the narrow-bandgap cells. To solve this conflict and identify the optimal bandgap, it is essential to evaluate the LCOS for the entire TPVES. As formulated in Eq. (8), the LCOS is dependent on the round-trip efficiency, CPE, CPP. Furthermore, our analysis incorporates the input electricity price—a critical yet frequently overlooked parameter that significantly influences the techno-economics of energy storage systems. By integrating these factors, this work builds a comprehensive model to identify the economically optimal bandgap and the lowest overall LCOS.

Fig. 12 illustrates the LCOS for an ideal TPVES system based-Si as a function of the TPV cell's bandgap and cost. The analysis is presented in Fig. 12 a-d, each corresponding to a different electricity input price, detailed data in Supplementary Table 2. In all scenarios, the LCOS shows a positive correlation with the cell cost, but this effect is relatively lower than changing bandgaps observed through contour lines. A distinct U-shaped dependence on the bandgap is observed, indicating the existence of an optimal bandgap that minimizes the LCOS. Specifically, the minimum achievable LCOS increases significantly with the rising cost of input electricity. At an electricity price of 0.01$/kWh, a minimum LCOS of 0.036$/kWh is achieved at a bandgap of 0.88 eV, shown in Fig. 12a. As the input price increases to 0.10$/kWh, the minimum LCOS rises to 0.223$/kWh, with the optimal bandgap shifting to a higher value of 1.17 eV, shown in Fig. 12d. This trend demonstrates that higher charging costs not only elevate the overall storage cost but also shift the optimal TPV cell design towards wider bandgap materials under the ideal TPVES.

To provide a comparative assessment of material selection, Fig. 13 presents the LCOS analysis for an ideal TPVES system based on FeSiB, detailed data in Supplementary Table 3 under identical conditions as the Si-based system shown in Fig. 12. Fig. 13a-d correspond to the same range of input electricity prices from $0.01/kWh to $0.10/kWh. While the FeSiB-based system shows the trends, LCOS increasing with input

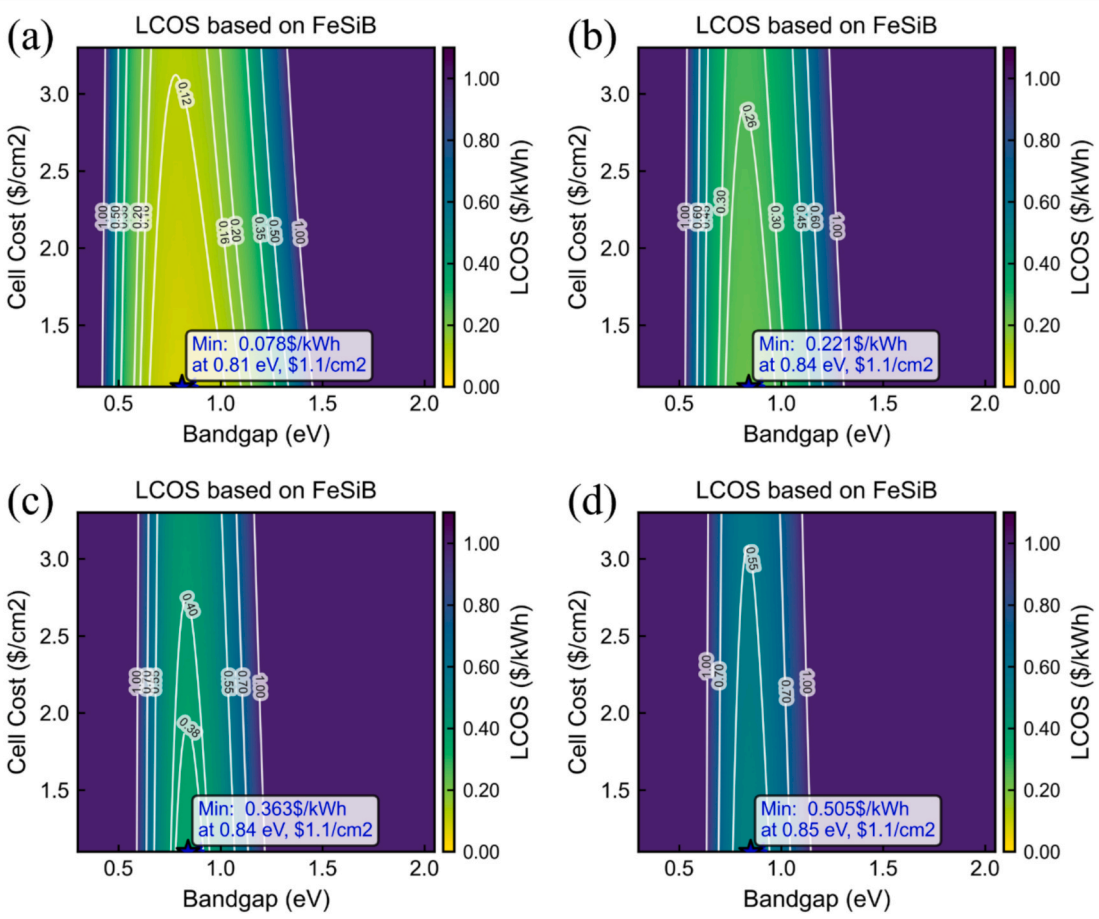

Fig.17. LCOS of the high quality TPVES system based on FeSiB under varying electricity input prices. (a) electricity of 0.01$/kWh, (b) electricity of 0.04$/kWh, (c) electricity of 0.07$/kWh, (d) electricity of 0.10$/kWh. Other parameters consistent with Fig. 16.

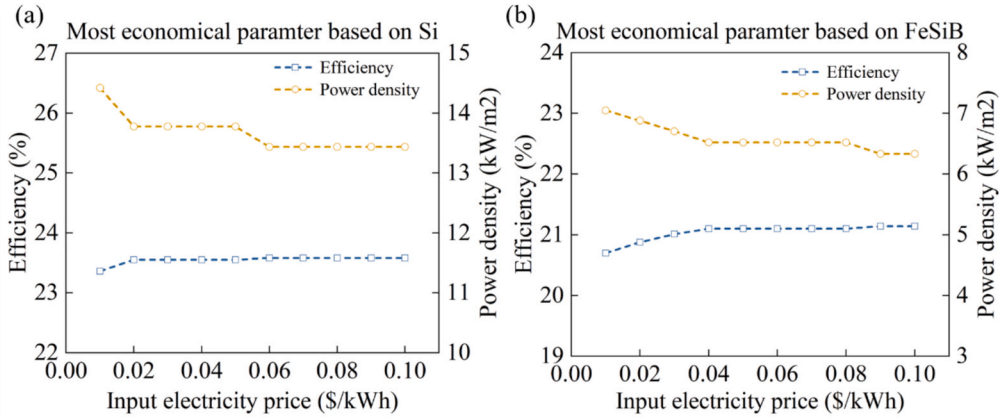

Fig.18. The most economical parameter of the high quality TPVES under varying electricity input prices. (a) the energy storage material uses Si, (b) the energy storage material uses FeSiB. Other parameters consistent with Fig. 16.

electricity price and the optimal bandgap shifting to higher energies, a direct comparison with the Si-based system reveals critical differences. Firstly, under all tested scenarios, the minimum achievable LCOS for the Si-based system is consistently lower than that of the FeSiB-based system (e.g., 0.036$/kWh for Si vs. 0.045$/kWh for FeSiB at an input price of $0.01/kWh). Secondly, the optimal bandgaps for the FeSiB system (ranging from 0.70 eV to 0.94 eV) are systematically lower than those for the Si system (0.88 eV to 1.17 eV).

To more clearly illustrate these findings, the optimal parameters derived from the detailed LCOS analyses are summarized in Fig. 14. This figure plots the most economical round-trip efficiency and power density as a direct function of the input electricity price for both Si-based and FeSiB-based systems. A crucial trend is immediately apparent: for both materials, the optimal efficiency exhibits a strong positive correlation with the input electricity price. For instance, in the Si-based system, the optimal efficiency rises from 43.06 % to 50.27 % as the electricity cost increases from $0.01/kWh to $0.10/kWh. Conversely, the optimal power density shows an inverse relationship. These plots

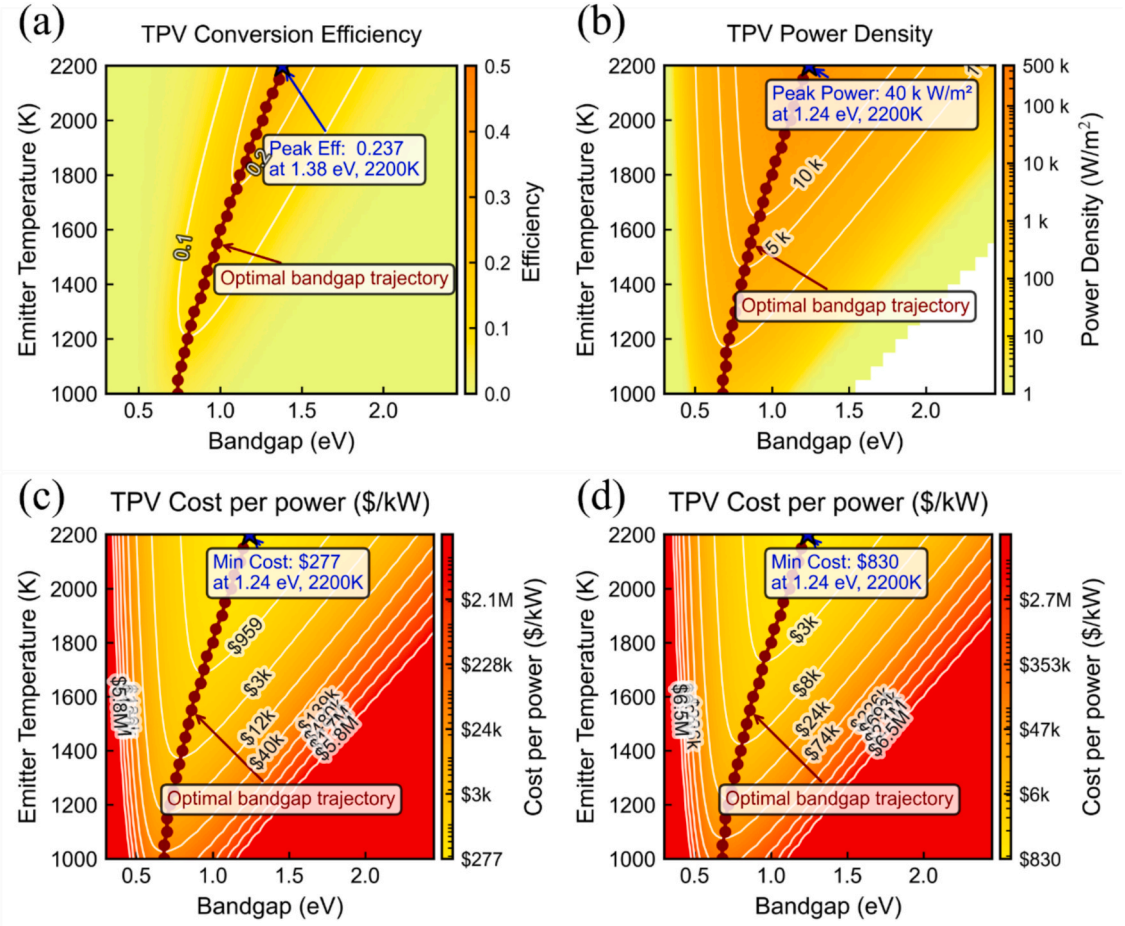

Fig. 19. Conversion efficiency, power density and CPP of intermediate quality TPV generator under varying bandgaps and emitter temperatures. (a) TPV conversion efficiency. (b) TPV power density. (c) CPP of TPV cell cost at \$1.1/cm^2; (d) CPP of TPV cell cost at \$3.3/cm^2. The high quality TPV parameters assume diode ideality factor of 1.15, R_s = 0.04 Ω·cm^2, R_{sh} = 10^2 Ω·cm^2, J_0 = 3000 × model, 95 % reflectance for sub-bandgap photons. Other parameters consistent with Fig. 11.

visually confirm that when input electricity is more expensive, maximizing energy utilization through higher efficiency becomes the dominant economic driver. Furthermore, Fig. 14 reinforces the superiority of the Si-based system, which consistently achieves both higher efficiencies and power densities compared to the FeSiB-based system across the entire price spectrum.

This comparative analysis suggests that, within the ideal framework of this study, Si holds a greater economic potential and that the optimal cell bandgap choice is intrinsically linked to the target operating conditions. The observed widening of the optimal bandgap reveals a key insight: as input electricity becomes more valuable, maximizing round-trip efficiency becomes a stronger economic driver. The model captures the trade-off between the higher-efficiency cells and the economic benefit of greater energy output. While this trade-off favors efficiency at higher electricity prices, its marginal utility diminishes as the escalating CPP begins to offset the efficiency gains. Ultimately, this comprehensive economic model provides a powerful methodology for identifying cost-minimizing bandgap materials under diverse operational and economic scenarios.

3.2.2. *High quality generator with storage system*

To evaluate the impact of practical physical limitations on TPV system performance, a comparative analysis is conducted between the high-quality TPV model, shown in Fig. 15, and the ideal model from Fig. 11. The high-quality model introduces more realistic physical constraints, including a non-zero series resistance (R_s=0.04 Ω·cm^2), a finite shunt resistance (R_{sh} = 10^3 Ω·cm^2), a higher dark current accounting for non-radiative recombination (J_0 = 3 × model), and 95 % sub-bandgap photon reflectance.

As expected, the introduction of these realistic factors leads to a significant reduction in all key performance metrics compared to the ideal model. The peak conversion efficiency drops sharply from a theoretical maximum of 62.4 % to a more practical value of 25.4 %, as shown in Fig. 15a. Similarly, the peak power density decreases from 240 kW/m^2 to 45 kW/m^2 shown in Fig. 15b. This performance degradation directly results in a substantial increase in the CPP. Fig. 15c presents that under the cell cost of 1.1\$/cm^2, the minimum cost rises from 46\$/kW to 209\$/kW.

The most critical and insightful finding from this comparative analysis is the convergence of the optimal bandgaps for different performance metrics (efficiency, power, and cost). As shown in Fig. 11, in the ideal model, a stark conflict exists between the bandgap for maximum efficiency at 2.24 eV and the bandgap for maximum power density at 0.58 eV, with a large gap of 1.66 eV. This presents a nearly irreconcilable design trade-off. However, in the high-quality model, this conflict is substantially mitigated. The optimal bandgap for achieving both peak power and minimum cost at 1.20 eV. Furthermore, the optimal bandgap for peak efficiency at 1.30 eV is now very close to this value, with a difference of only 0.1 eV. This convergence of optimal points has profound implications for practical device design. It demonstrates that for a well-designed, high-quality TPV system, it is no longer necessary to make an extreme trade-off between efficiency and power density. By selecting a single-junction material with a bandgap in the 1.2–1.3 eV range, it is possible to achieve near-optimal performance across all key

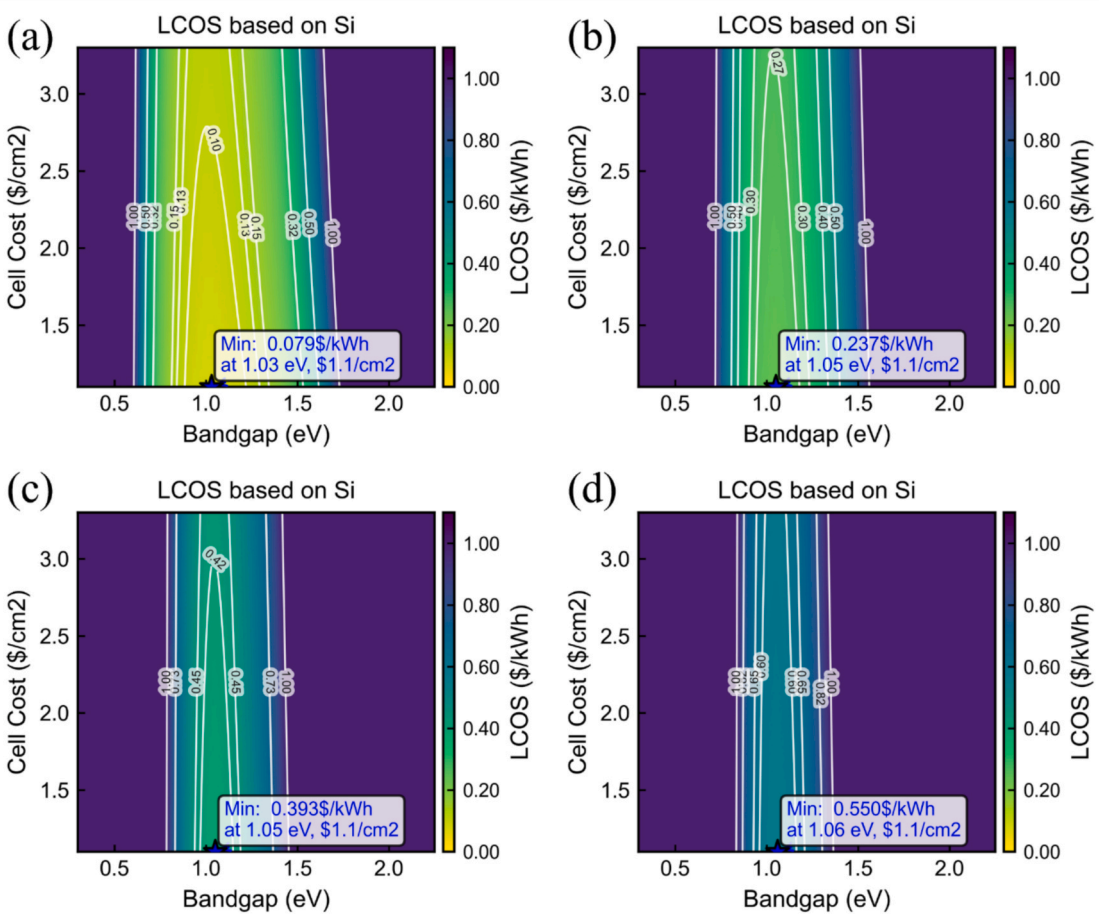

Fig. 20. LCOS of the intermediate quality TPVES system based on Si under varying electricity input prices. (a) electricity of 0.01$/kWh, (b) electricity of 0.04$/kWh, (c) electricity of 0.07$/kWh, (d) electricity of 0.10$/kWh. Simulations assume the system capacity of 100 MWh, reflector cost = 1.03$/m^2[88], discount rate of 7 %, system lifetime of 25 years, charging time of 5 h and discharging time of 10 h. [20,21,89]. Other parameters consistent with Fig. 19.

metrics simultaneously. This provides a feasible method for TPV design, which can achieve the consistency of efficiency and power density by adjusting the series resistance, shunt resistance and dark current of TPV cells.

To investigate the impact of physical device limitations on the TPVES system economics, Fig. 16 presents the LCOS analysis for the Si-based system under high quality model. A direct comparison with the ideal TPV reveals that these non-idealities lead to a significant increase in the system's LCOS. For instance, as shown in Fig. 16a, at an input electricity price of 0.01$/kWh, the minimum LCOS rises from 0.036$/kWh in the ideal model to 0.063$/kWh. This cost elevation persists across all electricity price scenarios, with the minimum LCOS increasing from $0.223/kWh to 0.446$/kWh at the 0.10$/kWh price point, presented in Fig. 16d. Furthermore, the presence of non-idealities also influences the optimal bandgap selection, shifting it from 0.88 eV in ideal model to 0.98 eV under low electricity prices. This analysis quantitatively demonstrates that performance losses in practical devices—such as resistive, non-radiative recombination, and optical losses—directly translate into a degradation of storage economics. It reveals that the critical importance of minimizing these loss mechanisms in future technological development to achieve cost-effective TPVES.

Fig. 17 applies high quality model parameters to the FeSiB-based TPVES system, aiming for a direct comparison with the high-quality TPV Si-based system. The results indicate that, like to the Si case, the LCOS of the high-quality FeSiB system increases substantially compared to its ideal model. At an input price of 0.01$/kWh, the minimum LCOS rises from an ideal value of 0.045$/kWh to 0.078$/kWh. More critically, the comparison with Fig. 16 reveals that the economic advantage of the Si-based system over the FeSiB-based system remains robust even when practical non-idealities are considered. Across all electricity price points, the minimum LCOS of the high-quality Si system is consistently lower than that of the high-quality FeSiB system. For instance, at the 0.01 $/kWh price point, the LCOS for the Si system (0.063$/kWh) is lower than that for the FeSiB system (0.078$/kWh). This cost advantage is maintained as the input electricity price increases. Furthermore, a notable phenomenon is observed when comparing the high quality TPVES model to its ideal model. In the high quality case, the optimal bandgap changes more slowly with the increasing input electricity price. This finding indicates that the LCOS of a high-performance TPVES is significantly less sensitive to the choice of the bandgap.

To provide a clear visual summary of these findings, Fig. 18 presents the optimal efficiency and power density for the high-quality TPVES as a function of input electricity price. The figure reveals a key distinction from the ideal case: the response of the optimal parameters to changing electricity prices is markedly suppressed. While a slight upward trend in efficiency is still observable for both Si and FeSiB, the curves are significantly flatter. This directly visualizes the conclusion that the economic optimization is less sensitive to parameter tuning when practical non-idealities are considered.

Consequently, this comparative analysis leads to a crucial conclusion: the economic superiority of Si as a TPV cell material persists through the transition from an ideal model to a more realistic high-quality model. This finding provides strong theoretical support for future material selection and research and development efforts.

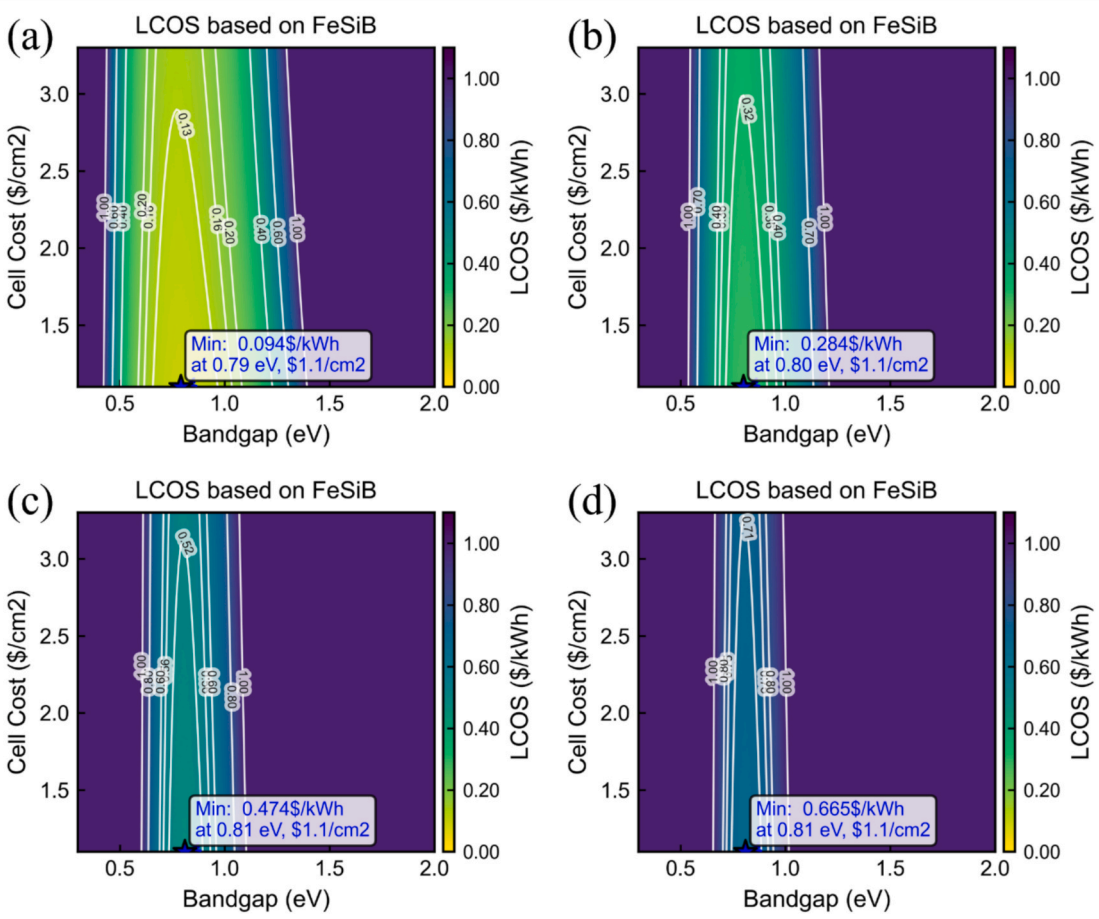

Fig. 21. LCOS of the intermediate quality TPVES system based on FeSiB under varying electricity input prices. (a) electricity of 0.01$/kWh, (b) electricity of 0.04 $/kWh, (c) electricity of 0.07$/kWh, (d) electricity of 0.10$/kWh. Other parameters consistent with Fig. 20.

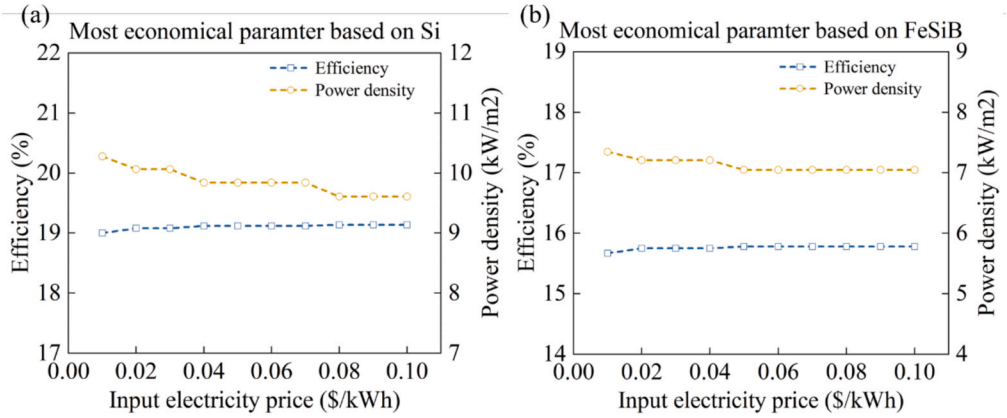

Fig. 22. The most economical parameter of the high quality TPVES under varying electricity input prices. (a) the energy storage material uses Si, (b) the energy storage material uses FeSiB. Other parameters consistent with Fig. 20.

3.2.3. Intermediate quality generator with storage system

To further investigate the effect of device imperfections on performance, Fig. 19 illustrates the characteristics of an intermediate quality TPV generator. Compared to the high-quality model, this model assumes further degradation in device parameters, which is more representative of potential process variations in real-world fabrication: the diode ideality factor is increased to 1.15, the shunt resistance is decreased to 10^2 $\Omega{\cdot}cm^2$, and the dark saturation current is also significantly larger.

Due to the lower device quality, all key performance metrics exhibit a further decline compared to the high-quality model. As shown in Fig. 19a, the peak conversion efficiency decreases from 25.4 % to 23.7 %, with its corresponding optimal bandgap at 1.38 eV. The peak power density drops from 45 kW/m^2 to 40 kW/m^2, as shown in Fig. 19b, with its optimal bandgap located at 1.24 eV. This performance degradation directly translates into higher costs. Assuming a cell cost of 1.1$/$cm^2$, the minimum CPP increases from 209$/kW for the high-quality model to 277$/kW, presented in Fig. 19c.

Interestingly, the optimal bandgap for peak efficiency at 1.38 eV

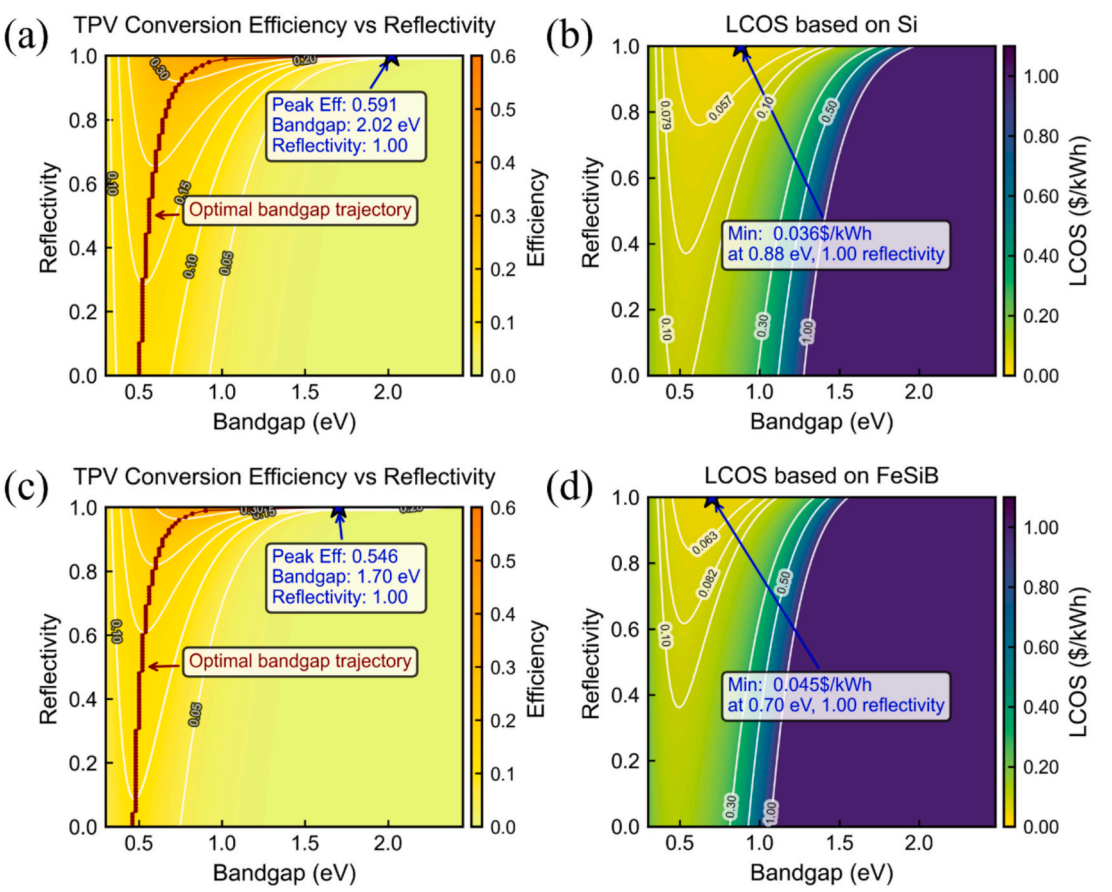

Fig. 23. Conversion efficiency and LCOS of ideal TPV generator under varying bandgaps and reflectivity. (a) TPV conversion efficiency based on Si. (b) LCOS of ideal TPVES based on Si. (c) TPV conversion efficiency based on FeSiB. (d) LCOS of ideal TPVES based on FeSiB. Simulations assume a blackbody emitter, TPV cell temperature fixed at 298 K, single-junction cells, 90 % quantum efficiency, unity view factor [21,87]. Economic parameters assume the system capacity of 100 MWh, electricity input price of 0.01$/kWh, reflector cost = 1.03$/m^2[88], TPV cell cost of 1.1$/cm^2, discount rate of 7 %, system lifetime of 25 years, charging time of 5 h and discharging time of 10 h. [20,89]. The ideal TPV parameters assume diode ideality factor of 1, $R_s = 0$ Ω·cm^2, $R_{sh} = 10^4$ Ω·cm^2, $J_0 = 1 \times$ model. The melting temperatures of Si and FeSiB are 1414 ℃ and 1157 ℃ respectively.

remains very close to this value of peak power density at 1.24 eV, with a difference of only 0.14 eV. This stands in stark contrast to the nearly irreconcilable 1.66 eV gap in the ideal model.

To further quantify the effect of cell quality on system cost, Fig. 20 presents the LCOS analysis for the Si-based system under an intermediate quality model. Compared to high quality model, the use of intermediate quality cells results in a further and significant growth of the system LCOS. At an input electricity price of 0.01$/kWh, as shown in Fig. 20a, the minimum LCOS increases from 0.063$/kWh in high quality TPV to 0.079$/kWh. This trend of cost increase is consistent across all electricity price scenarios, indicating that intensified internal losses within the cell directly and severely undermine the economic competitiveness of the TPVES system. Furthermore, the analysis shows that the degradation in cell quality also impacts the optimal design, with the optimal bandgap shifting slightly higher from 0.98 eV to 1.03 eV at 0.01 $/kWh electricity price. This figure provides evidence that TPV cell performance is a critical bottleneck determining the economic viability of the entire storage system, where even modest degradations in performance parameters lead to substantial cost increase.

Fig. 21 applies the intermediate quality model to the FeSiB based system, facilitating a final comparison with the Si-based system under equally realistic, lower-performance conditions. The analysis confirms that, consistent with all previous models, the Si-based system remains economically superior to the FeSiB-based system under intermediate quality conditions. At an input price of 0.01$/kWh, as shown in Fig. 21a, the minimum LCOS for the FeSiB system is 0.094$/kWh. This value is not only substantially higher than its costs in the ideal ($0.045/kWh) and high-quality ($0.078/kWh) models but is also significantly higher than the cost for the Si-based system ($0.079/kWh) under the same intermediate quality parameters. Although the optimal bandgap for the FeSiB system is consistently lower than that for the Si system, Si invariably demonstrates a lower LCOS within the scope of the techno-economic parameters explored in this study.

This conclusion is visually substantiated by Fig. 22, which illustrates the optimal parameters for the intermediate quality TPVES. The figure demonstrates an even more extreme flattening of the response curves compared to the previous models. For both Si and FeSiB, the optimal efficiency and power density are now almost completely insensitive to the input electricity price. This indicates that as cell quality decreases, the system's design optimum becomes entirely constrained by the need to manage severe internal losses, overriding any economic incentives from fluctuating energy costs. Most importantly, Fig. 22 provides a clear confirmation that the Si-based system maintains a robust advantage in both efficiency and power density, even under these lower-performance conditions.

3.2.4. *Sensitivity analysis*

To evaluate the influence of key parameters on the performance of the TPVES, a comprehensive sensitivity analysis is conducted. This analysis systematically investigated the individual effects of series resistance, EQE, CPE, charge and discharge times, and sub-bandgap photon reflectance. Among these, the main text provides a detailed

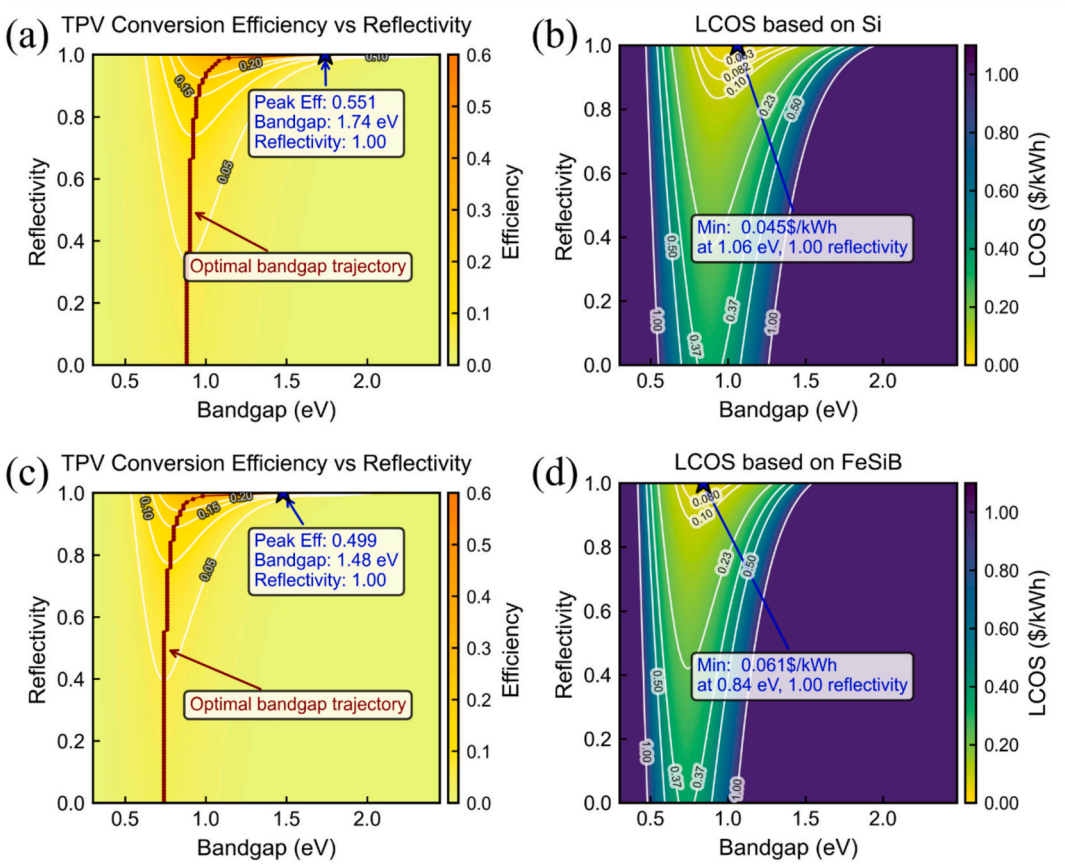

Fig. 24. Conversion efficiency and LCOS of high quality TPV generator under varying bandgaps and reflectivity. (a) TPV conversion efficiency based on Si. (b) LCOS of TPVES based on Si. (c) TPV conversion efficiency based on FeSiB. (d) LCOS of TPVES based on FeSiB. The high quality TPV parameters assume diode ideality factor of 1, $R_s = 0.04\ \Omega{\cdot}cm^2$, $R_{sh} = 10^3\ \Omega{\cdot}cm^2$, $J_0 = 3 \times$ model. Other parameters consistent with Fig. 23.

analysis of sub-bandgap photon reflectance on ideal, high-quality and intermediate-quality TPVES. The results for the other parameters—series resistance, EQE, CPE, charge time, and discharge time—are presented in the Supplementary Information Figs. S2–S6, respectively.

For sub-bandgap photon reflectance, Fig. 23 investigates the two-dimensional dependence of TPV conversion efficiency and the system's LCOS on cell bandgap and reflectivity. This analysis is conducted for ideal TPV models based on Si and FeSiB. As for TPV conversion efficiency, shown in Figs. 23a, c, the analysis clearly demonstrates that enhancing reflectivity is crucial for improving efficiency. This is attributed to the effective suppression of thermal losses via the recycling of unabsorbed sub-bandgap photons back to the heat source. In the ideal limit of 100 % reflectivity, the peak theoretical efficiencies for Si-based and FeSiB-based TPV cells can reach 59.1 % at a bandgap of 2.02 eV and 54.6 % at a bandgap of 1.70 eV respectively. Additionally, Optimal bandgap trajectory illustrates that as reflectivity decreases, the optimal bandgap for achieving maximum efficiency shifts towards lower energy values. This reveals that when photon recycling capabilities diminish, a cell with a narrower bandgap is required to re-optimize the trade-off between voltage loss and current gain. Furthermore, the relationship between the optimal bandgap and sub-bandgap reflectivity is highly nonlinear. The rightward shift of the optimal bandgap becomes more pronounced in the high-reflectivity regime. This acceleration occurs as sub-bandgap losses are suppressed, and minimizing thermalization losses by increasing the bandgap becomes the dominant optimization strategy. As shown in Figs. 23b, d, regarding system economics, the LCOS exhibits extreme sensitivity to reflectivity. High reflectivity boosts system efficiency, which reduces the energy loss, thereby significantly lowering the LCOS. At 100 % reflectivity, the minimum LCOS for the Si and FeSiB systems are 0.036$/kWh and 0.045$/kWh, respectively. These values are in perfect agreement with the results from the ideal models in Figs. 12 and 13, confirming that those previous analyses are based on the assumption of perfect photon recycling. Similar to the efficiency trend, the optimal bandgap for minimizing LCOS also decreases as reflectivity decreases.

In summary, sub-bandgap photon reflectivity is a paramount parameter governing both the performance and economic feasibility of a TPVES system. Furthermore, the optimal bandgap for a TPV cell is not a fixed value but a dynamic variable strongly coupled with the system's reflectivity. Under all comparable conditions, the Si-based system consistently demonstrates higher efficiency potential and a lower cost of storage than FeSiB-based TPVES.

Fig. 24 presents the reflectivity sensitivity analysis under a high quality TPV model, which evaluate how non-idealities in practical devices affect conversion efficiency and system economics through comparison with ideal TPV model. In contrast to the ideal TPV, this model introduces realistic physical limitations, including a non-zero series resistance (R_s=0.04 $\Omega{\cdot}cm^2$), shunt resistance (R_{sh}=$10^3\Omega{\cdot}cm^2$), and a higher dark saturation current (J_0=3 × model). Additionally, high quality TPV significantly degrade the system's optimal performance. As presented in Figs. 24a, c, the peak efficiency of the Si-based TPVES drops from an ideal 59.1 % to 55.1 % and that of the FeSiB-based TPVES decreases from 54.6 % to 49.9 %. This quantitatively reveals the performance penalty incurred by resistive and recombination losses. As for economic cost, Figs. 24b, d shows that the minimum LCOS for the Si-based system rises to 0.045$/kWh from an ideal 0.036$/kWh, while the FeSiB system's cost increases to 0.061$/kWh from 0.045$/kWh. Additionally, the presence of non-idealities alters the optimal bandgap selection. Interestingly, for achieving maximum efficiency, the optimal bandgap shifts to lower values from 2.02 eV to 1.74 eV for Si.

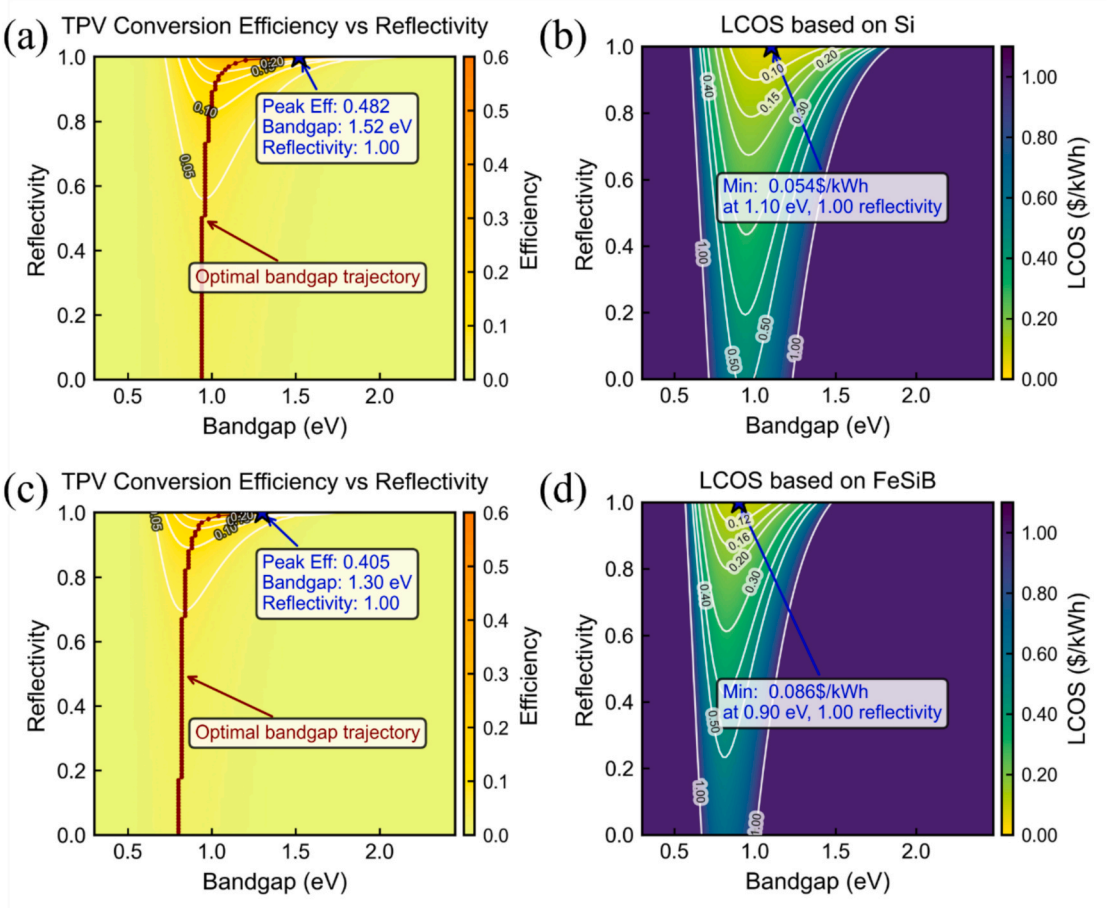

Fig. 25. Conversion efficiency and LCOS of intermediate quality TPV generator under varying bandgaps and reflectivity. (a) TPV conversion efficiency based on Si. (b) LCOS of TPVES based on Si. (c) TPV conversion efficiency based on FeSiB. (d) LCOS of TPVES based on FeSiB. The high quality TPV parameters assume diode ideality factor of 1.15, $R_s = 0.04\ \Omega{\cdot}cm^2$, $R_{sh} = 10^2\ \Omega{\cdot}cm^2$, $J_0 = 3000 \times$ model. Other parameters consistent with Fig. 23.

Conversely, for achieving minimum LCOS, the optimal bandgap shifts to higher values from 0.88 eV to 1.06 eV for Si. This reflects the more complex coupling between efficiency, cost, and bandgap in a more realistic physical model and reveals the comprehensive and superiority of model. Despite the degradation in performance, the fundamental trends persist. The analysis confirms that even within the high-quality model, (1) high reflectivity remains a prerequisite for achieving high efficiency and low cost, and (2) the optimal bandgap continues to shift to lower energies as reflectivity deteriorates.

Fig. 25 examines the impact of reflectivity on TPVES system performance and cost under an intermediate quality model. This model introduces more severe non-ideal parameters, including a higher diode ideality factor 1.15, a lower shunt resistance (R_{sh}=$10^2\ \Omega{\cdot}cm^2$), and a significantly higher dark saturation current (J_0=3000 × model). This analysis reveals the trend of progressive performance degradation with decreasing device quality. A clear performance decay trajectory can be observed when comparing with ideal and high quality TPV generator. Figs. 25a, c shows that the efficiency of the Si-based TPVES decreases from 59.1 % of ideal and 55.1 % of high quality down to 48.2 %. Similarly, the TPVES based on FeSiB drops from 54.6 % and 49.9 % to a final value of 40.5 %. Regarding cost, Figs. 25b, d illustrate the LCOS for the Si-based system rises from $0.036/kWh and $0.045/kWh to a final $0.054/kWh. Meanwhile, the LCOS for the FeSiB system climbs from $0.045/kWh and $0.061/kWh to $0.086/kWh. This coherent dataset compellingly demonstrates that the internal physical losses of the TPV cell are the significant factor limiting its economic viability. Moving from the ideal to the intermediate quality model, the LCOS for the Si system increases by 50 %, while the LCOS for the FeSiB system nearly 91 % increase.

A comprehensive analysis of the reflectivity sensitivity in ideal, high-Quality and intermediate-Quality model ensures that sub-bandgap photon reflectance is extremely significant for TPVES. The analyses consistently demonstrate that sub-bandgap photon reflectivity is the paramount parameter governing both the technical efficiency and economic feasibility of the system. Any degradation in reflectivity leads to a drastic deterioration in efficiency and a sharp increase in LCOS. Therefore, the development of near-perfect (R > 95 %) back-reflectors or optical filter structures is a fundamental prerequisite for the technology's path to commercialization.

3.2.5. *LCOS comparison between different EES*

To assess the economic feasibility of TPVES, a comparative analysis of its key economic parameters—CPE and CPP—is conducted against those of mainstream storage technologies. The specific results of this comparison are summarized in Supplementary Table 8 and further illustrated in diagrams for a more intuitive visual comparison. The detailed data is collected from previous peer-reviewed journals, websites and books. Considering the reported data for EES can vary significantly across literature sources—influenced by factors such as scale, geographical location, and technological maturity—the following figures are presented to encompass the full range of collected values. This approach ensures a comprehensive and objective comparison by illustrating the data spread for each technology rather than relying on single point-estimates.

As illustrated in Fig. 26, TPVES reveals a defining economic advantage, with a CPE range of approximately $4.95–$40/kWh, ranking it as

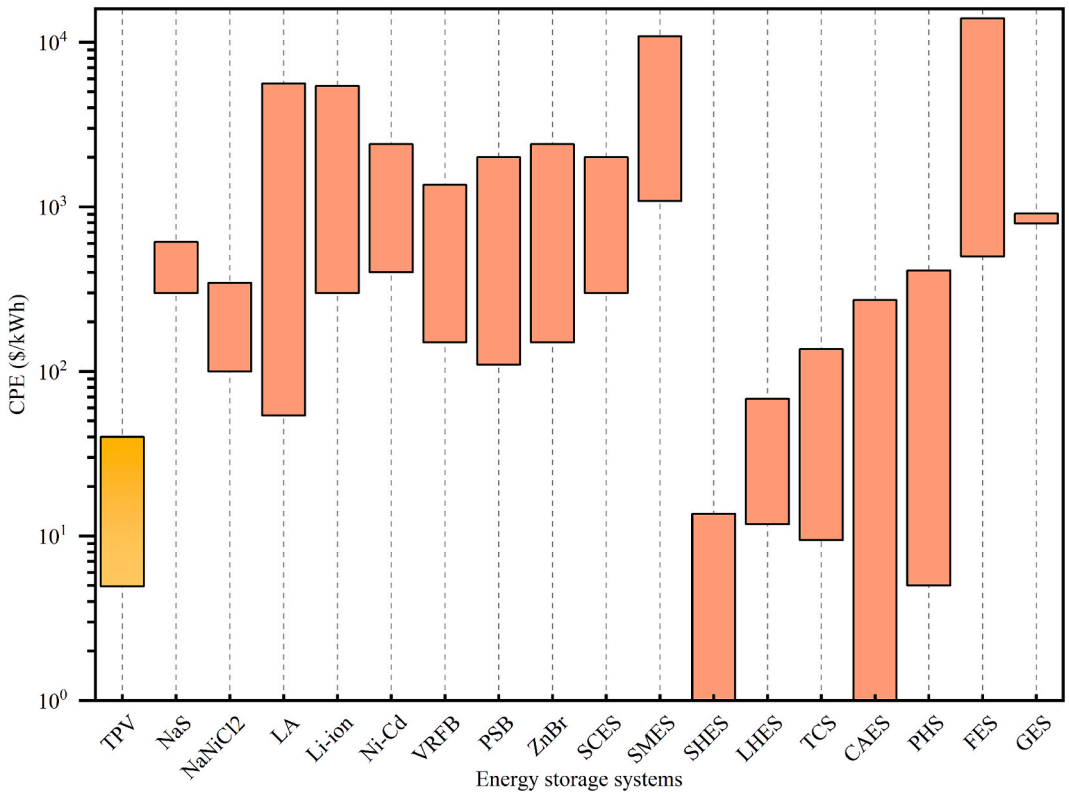

Fig. 26. CPE of TPV and selected energy storage systems. The detailed data are collected from: TPV [15,21], NaS [40,90,59], $NaNiCl_2$ [91,55], LA [46,90,40,59], Li-ion [92,49,59], Ni-Cd [93,42,46], VRFB [59,90,49], PSB [40,69,51], Zn Br [59,51,40,44,51], SCES [46], SMES [90], SHES [40,44,65], LHES [94,40,65], TCS [40,65], CAES [95,96,90,46], PHS[90,40,95,60], FES[90,55,46,49], GES [97].

one of the most cost-effective technologies. Specifically, the CPE for TPVES is one to two orders of magnitude lower than that of mainstream electrochemical batteries, such as Li-ion, LA, and VRFB. It is also significantly lower than mechanical storage systems like PHS and FES. Among all the technologies compared, the minimum achievable cost of TPVES is surpassed only by SHES and CAES. This exceptionally low CPE is a primary driver for TPVES achieving a competitive LCOS, confirming its significant potential for energy storage applications.

As shown in Fig. 27, TPVES demonstrates a competitive CPP. This advantage stems from its exceptionally high power density under high temperature operating conditions, which allows for a reduction in the required cell area per unit of power, thereby enabling a relatively low CPP. While the CPP of TPVES may be higher than some specialized power-centric systems like SMES or FES, it is considerably lower than many mainstream battery technologies, such as Li-ion. A favorable CPP is therefore critical for evaluating a technology's suitability for high-value, power-intensive markets.

The economic feasibility of an energy storage system is often evaluated by comparing its LCOS. This parameter is critically dependent on the price of input electricity, which usually has been overlook in previous studies. Conventional economic comparisons of EES often utilize a single off-peak price, such as 0.035$/kWh in China [100], this work expands scope enabling a comprehensive sensitivity analysis. Fig. 28 presents a LCOS analysis comparing TPVES with mainstream EES across a wide range of electricity prices (0.01–0.1$/kWh). This approach facilitates a comprehensive evaluation of the cost of TPVES under diverse scenarios, revealing a broader spectrum of potential applications. For fair comparison, the techno-economic parameters of competing storage systems are based on their optimal reported values, as summarized in Table 4. Technologies with high daily self-discharge rates (e.g., NaS, $NaNiCl_2$, SCES, and SMES) are excluded from this analysis. It should be noted that for TPVES, the optimal CPP and efficiency vary with electricity prices; therefore, its performance is represented as a range in the table. The specific data of TPVES at different electricity prices can be found in Supplementary Table 2, 4, 6.

The three orange curves illustrate the LCOS of different quality TPVES: the ideal model (Ideal-TPV), the high-quality model (HQ-TPV), and the medium-quality model (MQ-TPV), revealing the significant impact of TPV cell quality on system economics. The ideal-TPVES exhibits relatively low LCOS in whole electricity prices, demonstrating the immense potential of the technology. However, the cost increases significantly when practical physical limitations are introduced. The LCOS of the HQ-TPV is substantially higher than the ideal case, while the MQ-TPV is even more costly, surpassing all other EES at input electricity prices above 0.03$/kWh. This highlights the gap between theoretical promise and practical reality, indicating that cell efficiency and internal losses are the critical bottlenecks limiting the commercial feasibility of TPV storage.

The LCOS curve crossover points in Fig. 28 serve as critical decision-making criteria for EES selection. They represent the economic tipping points where one technology becomes more cost-effective than another. As for ideal-TPVES, it holds considerable potential in low-electricity-price environments. At an input price of 0.01$/kWh, the LCOS of TPVES is not only lower than the most of battery technologies—including Li-ion, Ni-Cd and various flow batteries (VRFB, PSB, Zn-Br)—but is also competitive with thermal energy storage and mechanical storage systems. The competitiveness owes to its low annualized capital and operation and maintenance (O&M) costs, which make its economic advantage in low-cost energy. However, the advantage diminishes as the electricity price rises. When the input electricity price reaches 0.10$/kWh, the LCOS for TPVES growths to 0.223$/kWh, exceeding all mainstream EES. For HQ-TPV and MQ-TPV systems, though they are less cost-effective than an ideal TPV system across the entire range of input electricity prices, still demonstrate a competitive advantage over conventional batteries, such as lithium-ion at a low electricity price of $0.01/kWh.

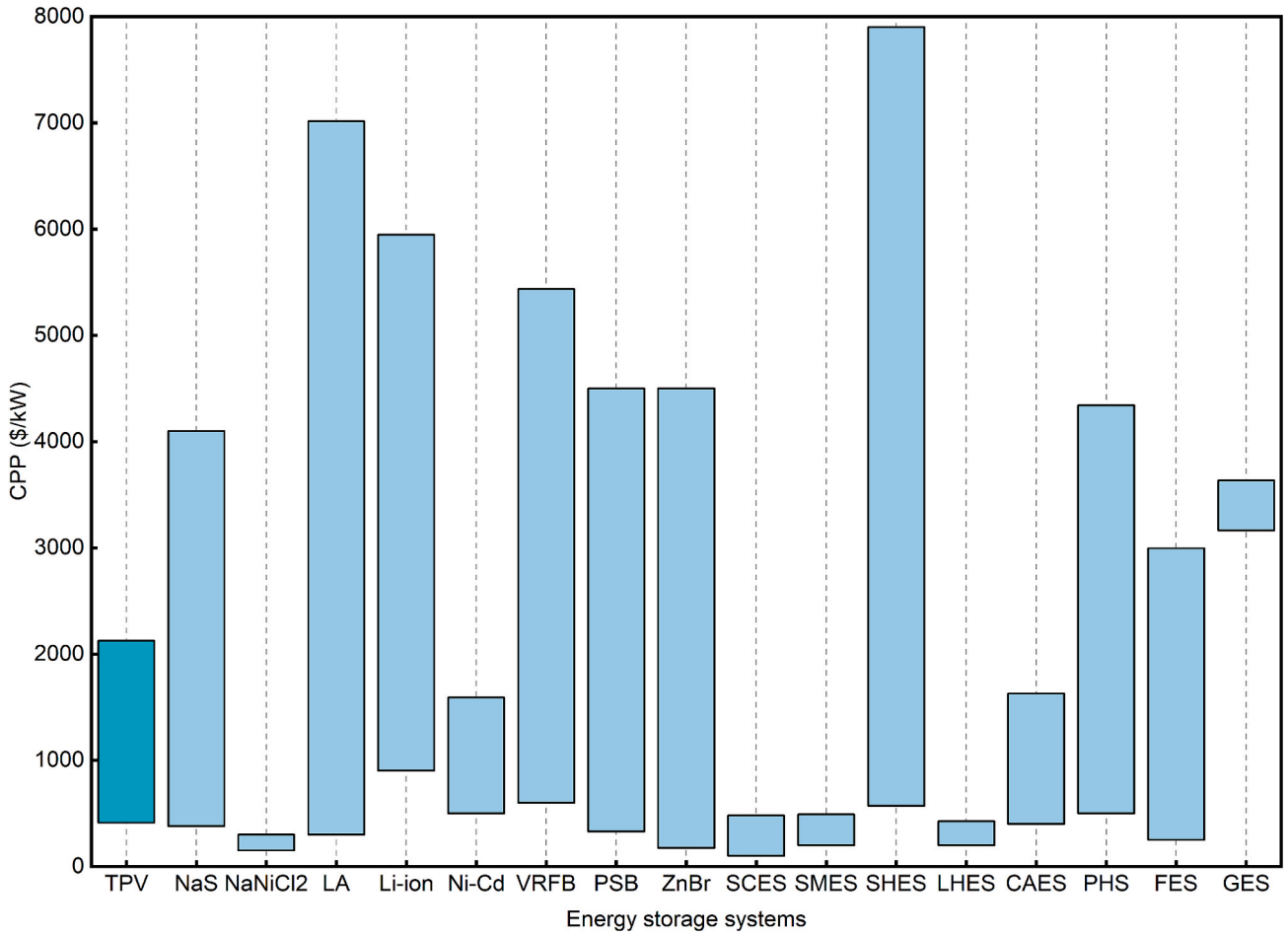

Fig. 27. CPP of TPV and selected energy storage systems. The detailed data are collected from: NaS [90,46,59], $NaNiCl_2$ [55], LA [46,90,49,59], Li-ion [98,49,59,46], Ni-Cd [93,46], VRFB [59,90,49], PSB [40,69,51], Zn Br [59,51,40,44], SCES [90,46], SMES [90,46], SHES [40,44,94], LHES [94,52], CAES [95,96,90,55], PHS [42,99,90,95,60], FES [59,90,40], GES [97].

A salient finding is that the LCOS curves for all TPV systems are the steepest among all technologies, visually representing their high sensitivity to input electricity prices. According to the fundamental principle of LCOS equation, this obvious slope is a direct indication of the system's relatively low round-trip efficiency. For TPVES, the reason is its extremely low conversion efficiency. Consequently, as the input electricity price rises, the financial cost associated with energy losses during the charge–discharge cycle is rapidly magnified.

The potential of TPVES becomes particularly evident when analyzing its ideal LCOS crossover points with other technologies. A critical intersection with Li-ion systems occurs at an electricity price of approximately 0.06$/kWh. While Li-ion's superior round-trip efficiency confers a cost advantage at higher prices, TPV is the more economical option below this threshold. This is highly significant in regions with low off-peak electricity rates, such as in China, where the price is $0.035/kWh [100]. At this price, an ideal TPVES is not only viable but also outperforms two-thirds of the battery systems evaluated in terms of LCOS. This finding indicates that if TPV technology can approach its theoretical performance limits, it has the potential to become a significant energy storage solution.

It is evident that the LCOS of TPVES is higher than that of both LHES and SHES across all electricity price scenarios. This appears somewhat contradictory, given that TPVES, as a novel thermal energy storage technology, is regarded as having significant potential. However, it is important to consider two key points when comparing systems. (1) LHES and SHES are typically analyzed under a combined heat and power model, which significantly enhances their overall energy utilization efficiency and thus lowers their levelized cost. In this study, our calculation of the LCOS for TPVES only accounts for the electricity-thermal-to-electric conversion, without considering the potential value of utilizing its waste heat. If a future TPVES design incorporate supplying thermal, its overall energy efficiency and cost competitiveness would be significantly improved. (2) While traditional thermal EES using technologies like the Rankine cycle may show a lower LCOS, they often require a large physical footprint and have longer response times, which can limit their flexibility in certain applications. TPVES, as a novel energy storage technology, offers a more compact design and faster response capabilities that are a significant advantage in real-world scenarios, and these benefits hold important value.

Furthermore, these crossover points indicates that there is no single universally optimal energy storage technology. The choice of the best technology is highly dependent on the specific application scenario and the local electricity market environment. For instance, in an area with abundant off-peak electricity resources, a storage technology with slightly lower round-trip efficiency but lower capital cost can be selected. In contrast, in a region with generally high electricity prices, high round-trip efficiency becomes the key factor determining the LCOS.

Therefore, TPV is not a universally applicable energy storage technology, but it has clear application potential in specific niche markets. Its economically viable range is strictly limited to scenarios with low or even zero cost heat or power sources. For example, it can be combined with industrial waste heat recovery, waste incineration, or the consumption of abandoned electricity from renewable energy sources (such as solar and wind power). In these scenarios, the extremely low input

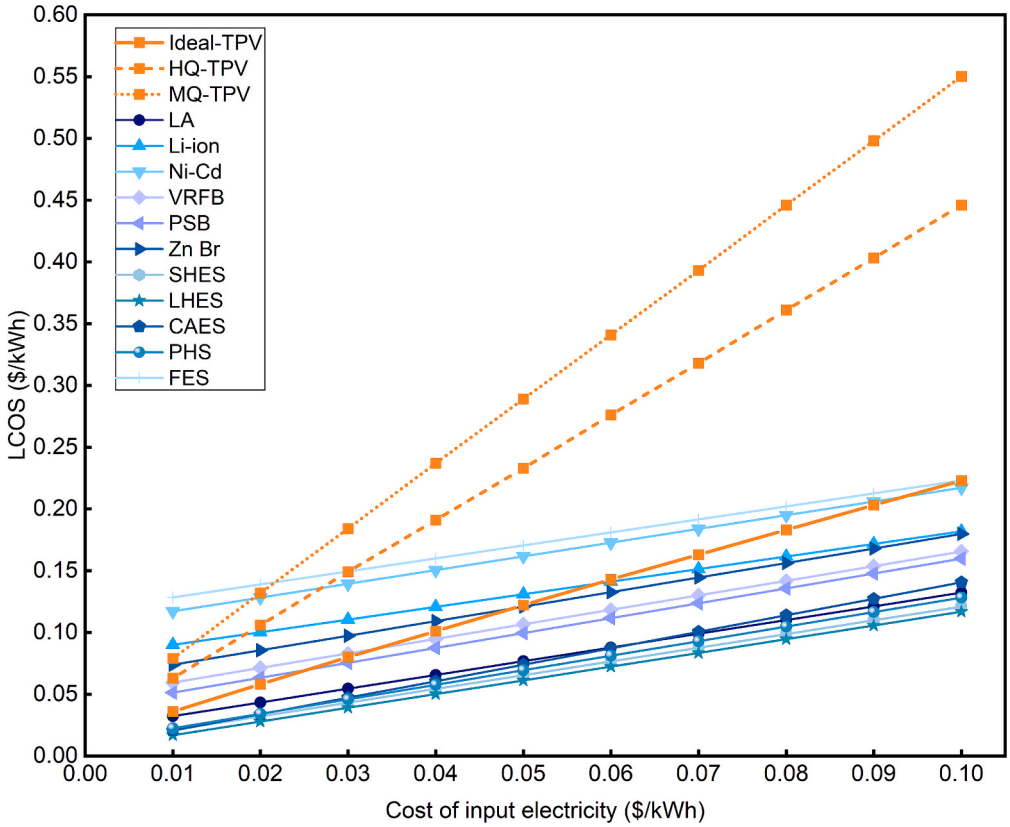

Fig. 28. LCOS of TPV and mainstream energy storage systems under different input electricity prices. Simulations assume the system capacity of 100 MWh, discount rate of 7 %, system lifetime of 25 years, reflector cost = 1.03$/m^2 [88], TPV cell cost of 1.1$/cm^2, charging time of 5 h and discharging time of 10 h [20,21,89].

Table 4
The values of input optimal techno-economic parameters of energy storage systems.

Type of ESDs	CPE ($/kWh)	CPP($/kW)	CPOM ($/kW/year)	Efficiency (%)	Service life (years)
Ideal-TPV	6.27	410.6–1257.2	16 [40,101]	43.06–50.27	25
HQ-TPV	6.27	762.9–818.8	16 [40,101]	23.36–23.58	25
MQ-TPV	6.27	1070.1–1144.7	16 [40,101]	19–19.14	25
LA	54	300	7 [102]	90	15
Li-ion	300	900	6 [102]	98	20
Ni-Cd	400	500	20 [42]	90	20
VRFB	150	600	7 [102]	85	20
PSB	110	330	7 [102]	83	15
Zn Br	150	175	6 [103]	85	10
SHES	0.04	571	18.5 [42]	90	30
LHES	11.78	200	5 [42]	90	40
CAES	1	400	16.7 [40]	75	50
PHS	5	500	6.2 [102]	85	60
FES	500	250	5.6 [40]	95	20

energy cost can maximize the advantage of its low capital cost while avoiding the negative impact of its low efficiency at high electricity prices.

4. Conclusion

This study provides a comprehensive techno-economic modeling and evaluation of TPVES, exploring its potential as a competitive alternative to existing large-scale energy storage technologies. By analyzing the influence of emitter temperature and cell bandgap on efficiency, power density, CPE, CPP, LCOS, we draw the following conclusions:

(1) This study establishes a robust, experimentally validated physics model, which subsequently enables a systematic exploration of the three quality TPV systems theoretical performance limits across a range of semiconductor bandgaps. The findings from this model-based analysis confirm that TPV holds strong potential as a high-performance and cost-effective solution for energy storage.
(2) Multi-dimensional simulations incorporating bandgap, temperature, and electricity input price identify optimal configurations that minimize LCOS. Through systematic model-based optimization, a significant reduction in the LCOS is demonstrated, achieving a value as low as 0.036$/kWh. This result is realized using 0.88 eV bandgap TPV materials under the condition of a 0.01$/kWh electricity price. These findings provide basis for the design of economically competitive TPV systems adaptable to diverse market conditions.
(3) This techno-economic analysis, which establishes electricity input price as a major variable, demonstrates the competitive edge of TPVES against numerous mainstream technologies. While its low round-trip efficiency is a limitation, TPVES exceptionally low energy media cost provides an advantage in low-price electricity scenarios. For instance, at a price below 0.035$/kWh—the off-peak tariff in China—ideal TPV achieves LCOS lower than two-thirds of competing battery systems and remains more cost-effective than Li-ion batteries with electricity below 0.06$/kWh. This combination of cost-effectiveness (CPE of 4.95–40$/kWh), high energy density, and long service life (20–25 years) positions TPV as an ideal solution for space-constrained and storing surplus renewable energy application.

Overall, this study demonstrates that TPVES represents a technically

feasible and economically competitive solution for future grid-scale applications, particularly for utilizing surplus energy sources. Despite these promising prospects, several significant challenges must be addressed to facilitate its widespread industrial adoption. A notable discrepancy persists between the ideal efficiencies in simulations and those achievable in practical and large-scale systems. Furthermore, ensuring long-term operational reliability—specifically maintaining the high-vacuum integrity between the emitter and the TPV cell to prevent oxidation of hot-end components over a multi-decade lifespan—remains a critical engineering hurdle. Effective thermal management strategies are also imperative to mitigate TPV cell temperature elevation during sustained operation, which can otherwise lead to performance degradation. Finally, the process of manufacturing presents a formidable challenge, as achieving high uniformity in material quality and thin-film thickness across large-area devices is essential to prevent mismatch losses that degrade overall system efficiency. Collectively, these issues highlight the key barriers that must be overcome for the future industrialization of TPVES.

A promising direction for future work is the integration of TPVES into cogeneration architectures, aiming to enhance overall energy utilization and economic feasibility for industrial or district-scale applications. Additionally, the present study is confined to a steady-state perspective. For a more realistic and comprehensive assessment, future investigations should aim to address the transient thermal response of the system and develop a grid-integration model that accounts for the fluctuations in electricity markets. Incorporating dynamic electricity pricing is essential for formulating optimal dispatch strategies and accurately evaluating the economic performance of such integrated systems.

CRediT authorship contribution statement

Wuyong Qu: Writing – original draft, Visualization, Validation, Software, Methodology, Conceptualization. **Haoming Li:** Writing – review & editing, Writing – original draft, Validation, Software, Methodology. **Zhiyuan Zhou:** Writing – original draft, Visualization. **Guangyao Li:** Writing – review & editing, Visualization. **Neven Duić:** Writing – review & editing. **Dongxu Ji:** Writing – review & editing, Supervision, Resources, Project administration, Funding acquisition.

Declaration of competing interest

The authors declare that they have no known competing financial interests or personal relationships that could have appeared to influence the work reported in this paper.

Acknowledgments

This work is financially supported by the National Natural Science Foundation of China (Grant No. 52576233) and Shenzhen Science and Technology Innovation Commission (Grant No. KCXST20221021111609024, JCYJ20220818103010021).

Appendix A. Supplementary data

Supplementary data to this article can be found online at https://doi.org/10.1016/j.enconman.2025.120739.

Data availability

Data will be made available on request.

References

[1] Ali HM, Rehman T, Arıcı M, Said Z, Duraković B, Mohammed HI, et al. Advances in thermal energy storage: fundamentals and applications. Prog. Energy Combust. Sci. 2024;100:101109. https://doi.org/10.1016/j.pecs.2023.101109.
[2] Xie J, Xia Y, Liang L, Zhang W, Shi M. Pricing strategy for renewable energy source electricity in the competitive hybrid electricity market. Ind. Manag. Amp Data Syst. 2018;118:1071–93. https://doi.org/10.1108/IMDS-08-2017-0341.
[3] Tan KM, Babu TS, Ramachandaramurthy VK, Kasinathan P, Solanki SG, Raveendran SK. Empowering smart grid: a comprehensive review of energy storage technology and application with renewable energy integration. J Energy Storage 2021;39:102591. https://doi.org/10.1016/j.est.2021.102591.
[4] Chen M, Zhang Y, Xing G, Chou S-L, Tang Y. Electrochemical energy storage devices working in extreme conditions. Energy Environ. Sci. 2021;14:3323–51. https://doi.org/10.1039/D1EE00271F.
[5] Showers SO, Raji AK. Benefits and challenges of energy storage technologies in high penetration renewable energy power systems. IEEE PESIAS PowerAfrica 2019;2019:209–14. https://doi.org/10.1109/PowerAfrica.2019.8928644.
[6] Jiang T, Shen D, Zhang Z, Liu H, Zhao G, Wang Y, et al. Battery technologies for grid-scale energy storage. Nat. Rev. Clean Technol. 2025:1–19. https://doi.org/10.1038/s44359-025-00067-9.
[7] Mahmoud M, Ramadan M, Olabi A-G, Pullen K, Naher S. A review of mechanical energy storage systems combined with wind and solar applications. Energy Convers Manag 2020;210:112670. https://doi.org/10.1016/j.enconman.2020.112670.
[8] Sadeghi G. Energy storage on demand: thermal energy storage development, materials, design, and integration challenges. Energy Storage Mater. 2022;46:192–222. https://doi.org/10.1016/j.ensm.2022.01.017.
[9] Review of organic Rankine cycle for small-scale applications. Energy Convers. Manag. 2017;134:135–55. https://doi.org/10.1016/j.enconman.2016.12.023.
[10] Zare S, Tavakolpour-Saleh A. Free piston stirling engines: a review. Int. J. Energy Res. 2020;44:5039–70. https://doi.org/10.1002/er.4533.
[11] Tohidi F, Holagh SG, Chitsaz A. Thermoelectric generators: a comprehensive review of characteristics and applications. Appl. Therm. Eng. 2022;201:117793. https://doi.org/10.1016/j.applthermaleng.2021.117793.
[12] Datas A, Ramos A, Martí A, Del Cañizo C, Luque A. Ultra high temperature latent heat energy storage and thermophotovoltaic energy conversion. Energy 2016;107:542–9. https://doi.org/10.1016/j.energy.2016.04.048.
[13] LaPotin A, Schulte KL, Steiner MA, Buznitsky K, Kelsall CC, Friedman DJ, et al. Thermophotovoltaic efficiency of 40%. Nature 2022;604:287–91. https://doi.org/10.1038/s41586-022-04473-y.
[14] Roy-Layinde B, Lim J, Arneson C, Forrest SR, Lenert A. High-efficiency air-bridge thermophotovoltaic cells. Joule 2024;8:2135–45. https://doi.org/10.1016/j.joule.2024.05.002.
[15] Amy C, Seyf HR, Steiner MA, Friedman DJ, Henry A. Thermal energy grid storage using multi-junction photovoltaics. Energy Environ. Sci. 2019;12:334–43. https://doi.org/10.1039/C8EE02341G.
[16] C.C. Kelsall, K. Buznitsky, A. Henry, Technoeconomic Analysis of Thermal Energy Grid Storage Using Graphite and Tin 2021. Doi: 10.48550/arXiv.2106.07624.
[17] Li H, Wan S, Wang L, Zhao J, Ji D. Divide and conquer: Spectral-splitting and utilization of thermal radiation from waste heat in the steel industry. Appl. Energy 2025;378:124836. https://doi.org/10.1016/j.apenergy.2024.124836.
[18] Lenert A, Bierman DM, Nam Y, Chan WR, Celanović I, Soljačić M, et al. A nanophotonic solar thermophotovoltaic device. Nat. Nanotechnol. 2014;9:126–30. https://doi.org/10.1038/nnano.2013.286.
[19] Verma S, Buznitsky K, Henry A. Thermophotovoltaic performance metrics and techno-economics: efficiency vs. power density. Appl. Energy 2025;384:125479. https://doi.org/10.1016/j.apenergy.2025.125479.
[20] Datas A, Bondavalli P, Pantaleo AM. Embracing thermophotovoltaic electricity: pathways to market adoption. Sol. Energy Mater. Sol. Cells 2025;283:113419. https://doi.org/10.1016/j.solmat.2025.113419.
[21] Datas A, López-Ceballos A, López E, Ramos A, Del Cañizo C. Latent heat thermophotovoltaic batteries. Joule 2022;6:418–43. https://doi.org/10.1016/j.joule.2022.01.010.
[22] Sakr M, Liu S. A comprehensive review on applications of ohmic heating (OH). Renew. Sustain. Energy Rev. 2014;39:262–9. https://doi.org/10.1016/j.rser.2014.07.061.
[23] V. Rudnev, D. Loveless, R.L. Cook, Handbook of induction heating 2nd ed. 2017, CRC Press Boca, Raton, Doi: 10.1201/9781315117485.
[24] Metaxas AC, Meredith RJ. Industrial microwave heating. IET 1983.
[25] Wang G, Tang Z, Gao Y, Liu P, Li Y, Li A, et al. Phase Change thermal storage materials for interdisciplinary applications. Chem. Rev. 2023;123:6953–7024. https://doi.org/10.1021/acs.chemrev.2c00572.
[26] Gamel MMA, Lee HJ, Rashid WESWA, Ker PJ, Yau LK, Hannan MA, et al. A review on thermophotovoltaic cell and its applications in energy conversion. Issues Recommend. Mater. 2021;14:4944. https://doi.org/10.3390/ma14174944.
[27] Tuley RS, Nicholas RJ. Band gap dependent thermophotovoltaic device performance using the InGaAs and InGaAsP material system. J. Appl. Phys. 2010;108:084516. https://doi.org/10.1063/1.3488903.
[28] Kocher JD, Woods J, Odukomaiya A, Mahvi A, Yee SK. Thermal battery cost scaling analysis: minimizing the cost per kW h. Energy Environ. Sci. 2024;17:2206–18. https://doi.org/10.1039/D3EE03594H.
[29] Datas A. Ultra high temperature thermal energy storage for dispatchable power generation. Elsevier 2022:141–50. https://doi.org/10.1016/B978-0-12-819723-3.00088-3.

[30] Jiao J, Grorud B, Sindland C, Safarian J, Tang K, Sellevoll K, et al. The use of Eutectic Fe-Si-B alloy as a phase change material in thermal energy storage systems. Materials 2019;12:2312. https://doi.org/10.3390/ma12142312.
[31] Amy C, Kelsall CC, LaPotin A, Pishahang M, Henry A. Chapter 3 - Ultrahigh temperature sensible heat storage and heat transfer fluids. In: Datas A, editor. Ultra-High Temp. Therm. Energy Storage Transf. Convers., Woodhead Publishing; 2021, p. 57–84. Doi: 10.1016/B978-0-12-819955-8.00003-X.
[32] Lang S, Drück H, Bestenlehner D. Chapter 8 - Ultrahigh temperature thermal insulation. In: Datas A, editor. Ultra-High Temp. Therm. Energy Storage Transf. Convers., Woodhead Publishing; 2021, p. 201–19. Doi: 10.1016/B978-0-12-819955-8.00008-9.
[33] Chan W, Huang R, Wang C, Kassakian J, Joannopoulos J, Celanovic I. Modeling low-bandgap thermophotovoltaic diodes for high-efficiency portable power generators. Sol. Energy Mater. Sol. Cells 2010;94:509–14. https://doi.org/10.1016/j.solmat.2009.11.015.
[34] Omair Z, Scranton G, Pazos-Outón LM, Xiao TP, Steiner MA, Ganapati V, et al. Ultraefficient thermophotovoltaic power conversion by band-edge spectral filtering. Proc. Natl. Acad. Sci. 2019;116:15356–61. https://doi.org/10.1073/pnas.1903001116.
[35] Lee B, Lentz R, Burger T, Roy-Layinde B, Lim J, Zhu RM, et al. Air-bridge Si thermophotovoltaic cell with high photon utilization. ACS Energy Lett. 2022;7:2388–92. https://doi.org/10.1021/acsenergylett.2c01075.
[36] Cappelletti MA, Casas GA, Cédola AP, Peltzer y Blancá EL, Marí, Soucase B. Study of the reverse saturation current and series resistance of p-p-n perovskite solar cells using the single and double-diode models. Superlattice. Microst. 2018;123:338–48. https://doi.org/10.1016/j.spmi.2018.09.023.
[37] Somasundaran P, Gupta R. Evaluation of shunt losses in industrial silicon solar cells. Int. J. Photoenergy 2016;2016:8029608. https://doi.org/10.1155/2016/8029608.
[38] Singh P, Ravindra NM. Temperature dependence of solar cell performance—an analysis. Sol. Energy Mater. Sol. Cells 2012;101:36–45. https://doi.org/10.1016/j.solmat.2012.02.019.
[39] Xu J, Zhou C, Li W. Photovoltaic single diode model parameter extraction by d*I*/d*V*-assisted deterministic method. Sol. Energy 2023;251:30–8. https://doi.org/10.1016/j.solener.2023.01.009.
[40] Kebede AA, Kalogiannis T, Van Mierlo J, Berecibar M. A comprehensive review of stationary energy storage devices for large scale renewable energy sources grid integration. Renew. Sustain. Energy Rev. 2022;159:112213. https://doi.org/10.1016/j.rser.2022.112213.
[41] Akhil AA, Huff G, Currier AB, Hernandez J, Bender DA, Kaun BC, et al. DOE/EPRI Electricity Storage Handbook in Collaboration with NRECA. Sandia National Lab. (SNL-NM), Albuquerque, NM (United States); Electric Power Research Inst. (EPRI), Palo Alto, CA (United States); 2016. Doi: 10.2172/1431469.
[42] Luo X, Wang J, Dooner M, Clarke J. Overview of current development in electrical energy storage technologies and the application potential in power system operation. Appl. Energy 2015;137:511–36. https://doi.org/10.1016/j.apenergy.2014.09.081.
[43] Li L, Wang B, Jiao K, Ni M, Du Q, Liu Y, et al. Comparative techno-economic analysis of large-scale renewable energy storage technologies. Energy AI 2023;14:100282. https://doi.org/10.1016/j.egyai.2023.100282.
[44] Díaz-González F, Sumper A, Gomis-Bellmunt O, Villafáfila-Robles R. A review of energy storage technologies for wind power applications. Renew. Sustain. Energy Rev. 2012;16:2154–71. https://doi.org/10.1016/j.rser.2012.01.029.
[45] Farret FA, Simões MG. Integration of Alternative Sources of Energy, Vol. 504. Piscataway, NJ, USA: IEEE press; 2006.
[46] Das CK, Bass O, Kothapalli G, Mahmoud TS, Habibi D. Overview of energy storage systems in distribution networks: placement, sizing, operation, and power quality. Renew. Sustain. Energy Rev. 2018;91:1205–30. https://doi.org/10.1016/j.rser.2018.03.068.
[47] McCluer, S., & Christin, J.-F. (2011). Comparing data center batteries, flywheels, and ultracapacitors (White Paper 65, Rev. 2). Schneider Electric. https://www.apcbj.com/pdf/DBOY-77FNCT_R2_EN.pdf.
[48] Zhu WH, Zhu Y, Davis Z, Tatarchuk BJ. Energy efficiency and capacity retention of Ni–MH batteries for storage applications. Appl. Energy 2013;106:307–13. https://doi.org/10.1016/j.apenergy.2012.12.025.
[49] Rohit AK, Rangnekar S. An overview of energy storage and its importance in Indian renewable energy sector: Part II – energy storage applications, benefits and market potential. J. Energy Storage 2017;13:447–56. https://doi.org/10.1016/j.est.2017.07.012.
[50] Beaudin M, Zareipour H, Schellenberglabe A, Rosehart W. Energy storage for mitigating the variability of renewable electricity sources: an updated review. Energy Sustain. Dev. 2010;14:302–14. https://doi.org/10.1016/j.esd.2010.09.007.
[51] Bradbury K. Energy storage technology review kyle bradbury. 2010. https://www.kylebradbury.org/docs/papers/Energy-Storage-Technology-Review-Kyle-Bradbury-2010.pdf.
[52] Chen H, Cong TN, Yang W, Tan C, Li Y, Ding Y. Progress in electrical energy storage system: a critical review. Prog. Nat. Sci. 2009;19:291–312. https://doi.org/10.1016/j.pnsc.2008.07.014.
[53] Kondoh J, Ishii I, Yamaguchi H, Murata A, Otani K, Sakuta K, et al. Electrical energy storage systems for energy networks. Energy Convers Manag 2000;41:1863–74. https://doi.org/10.1016/S0196-8904(00)00028-5.
[54] EPRI-DOE Handbook of Energy Storage for Transmission &Distribution Applications, EPRI, Palo Alto, CA, and the U.S. Department of Energy, Washington, DC: 2003, 1001834.
[55] Aneke M, Wang M. Energy storage technologies and real life applications – a state of the art review. Appl. Energy 2016;179:350–77. https://doi.org/10.1016/j.apenergy.2016.06.097.
[56] L. de Sousa (2011, October 5). Energy storage - flywheel. The Oil Drum. http://theoildrum.com/node/8428.
[57] Gyuk, I., Johnson, M., Vetrano, J., Lynn, K., Parks, W., Handa, R., & Braccio, R. (2013). Grid energy storage. US Department of Energy.
[58] Giteau M, Picardi MF, Papadakis GT. Thermodynamic figure of merit for thermophotovoltaics. J. Photonics Energy 2024;14. https://doi.org/10.1117/1.JPE.14.042402.
[59] Emrani A, Berrada A. A comprehensive review on techno-economic assessment of hybrid energy storage systems integrated with renewable energy. J Energy Storage 2024;84:111010. https://doi.org/10.1016/j.est.2024.111010.
[60] Rahman MM, Oni AO, Gemechu E, Kumar A. Assessment of energy storage technologies: a review. Energy Convers Manag 2020;223:113295. https://doi.org/10.1016/j.enconman.2020.113295.
[61] Matheys J, Timmermans J-M, Van Mierlo J, Meyer S. Peter Van den Bossche. Comparison of the environmental impact of five electric vehicle battery technologies using LCA. Int J Sustain Manuf 2009;1:318–29. https://doi.org/10.1504/IJSM.2009.023977.
[62] Vazquez S, Lukic SM, Galvan E, Franquelo LG, Carrasco JM. Energy storage systems for transport and grid applications. IEEE Trans. Ind. Electron. 2010;57:3881–95. https://doi.org/10.1109/TIE.2010.2076414.
[63] Zhao P, Zhang H, Zhou H, Chen J, Gao S, Yi B. Characteristics and performance of 10kW class all-vanadium redox-flow battery stack. J. Power Sources 2006;162:1416–20. https://doi.org/10.1016/j.jpowsour.2006.08.016.
[64] G.P. Rajarathnam, The Zinc/Bromine Flow Battery: Fundamentals and Novel Materials for Technology Advancement. PhD Thesis, 2016.
[65] Sarbu I, Sebarchievici C. A comprehensive review of thermal energy storage. Sustainability 2018;10(1):191. https://doi.org/10.3390/su10010191.
[66] Aziz MBA, Zain ZM, Baki SRMS, Muslam MN. Review on performance of Thermal Energy Storage system at S & T Complex, UiTM Shah Alam, Selangor. 2010 IEEE Control Syst. Grad. Res. Colloq. ICSGRC 2010, 2010, p. 49–54. Doi: 10.1109/ICSGRC.2010.5562524.
[67] Palizban O, Kauhaniemi K. Energy storage systems in modern grids—Matrix of technologies and applications. J Energy Storage 2016;6:248–59. https://doi.org/10.1016/j.est.2016.02.001.
[68] Ozcan H, El-Emam RS, Horri BA. Thermochemical looping technologies for clean hydrogen production – current status and recent advances. J. Clean. Prod. 2023;382:135295. https://doi.org/10.1016/j.jclepro.2022.135295.
[69] Hedegaard K, Meibom P. Wind power impacts and electricity storage – a time scale perspective. Renew. Energy 2012;37:318–24. https://doi.org/10.1016/j.renene.2011.06.034.
[70] Shin K, Lee J-H, Heo J, Kim H-T. Current status and challenges for practical flowless Zn–Br batteries. Curr. Opin. Electrochem. 2022;32:100898. https://doi.org/10.1016/j.coelec.2021.100898.
[71] Divya KC, Østergaard J. Battery energy storage technology for power systems—An overview. Electr. Pow. Syst. Res. 2009;79:511–20. https://doi.org/10.1016/j.epsr.2008.09.017.
[72] Hall PJ, Bain EJ. Energy-storage technologies and electricity generation. Energy Policy 2008;36:4352–5. https://doi.org/10.1016/j.enpol.2008.09.037.
[73] Sharma A, Tyagi VV, Chen CR, Buddhi D. Review on thermal energy storage with phase change materials and applications. Renew. Sustain. Energy Rev. 2009;13:318–45. https://doi.org/10.1016/j.rser.2007.10.005.
[74] Zalba B, Marín JM, Cabeza LF, Mehling H. Review on thermal energy storage with phase change: materials, heat transfer analysis and applications. Appl. Therm. Eng. 2003;23:251–83. https://doi.org/10.1016/S1359-4311(02)00192-8.
[75] Chinna Alluraiah N, Nandagopal V, Veeramanikandan P, Godfrey D, Meena S, Brindha G. Comparison of SoC in Ni-MH and Lithium-Ion battery for E Vehicle. IJEER 2024;12(4):1258–63. https://doi.org/10.37391/IJEER.120417.
[76] Connolly, D. (2010). A Review of Energy Storage Technologies: For the integration of fluctuating renewable energy. https://vbn.aau.dk/ws/portalfiles/portal/100570335/Energy_Storage_Techniques_v4.1.pdf.
[77] Alghamdi NS, Rana M, Peng X, Huang Y, Lee J, Hou J, et al. Zinc–Bromine rechargeable batteries: from device configuration, electrochemistry, material to performance evaluation. Nano-Micro Lett. 2023;15:209. https://doi.org/10.1007/s40820-023-01174-7.
[78] Forsberg CW, Stack DC, Curtis D, Haratyk G, Sepulveda NA. Converting excess low-price electricity into high-temperature stored heat for industry and high-value electricity production. Electr. J. 2017;30:42–52. https://doi.org/10.1016/j.tej.2017.06.009.
[79] Stack DC. Conceptual design and performance characteristics of firebrick resistance-heated energy storage for industrial heat supply and variable electricity production, 2017.
[80] Nelson RE. A brief history of thermophotovoltaic development. Semicond. Sci. Technol. 2003;18:S141. https://doi.org/10.1088/0268-1242/18/5/301.
[81] Coutts TJ. A review of progress in thermophotovoltaic generation of electricity. Renew. Sustain. Energy Rev. 1999;3:77–184.
[82] Feng D, Yee SK, Zhang ZM. Improved performance of a near-field thermophotovoltaic device by a back gapped reflector. Sol. Energy Mater. Sol. Cells 2022;237:111562. https://doi.org/10.1016/j.solmat.2021.111562.
[83] Tsvetkov N, Lee M, Kim Y, Kim D, Yun JS, Min H. Advancements in perovskite solar cell concentrators and future prospects. J. Mater. Chem. A 2025;13:7656–81. https://doi.org/10.1039/D4TA08688K.
[84] B. Dunbar R, C. Duck B, Moriarty T, F. Anderson K, W. Duffy N, J. Fell C, et al. How reliable are efficiency measurements of perovskite solar cells? The first inter-

comparison, between two accredited and eight non-accredited laboratories. J. Mater. Chem. A 2017;5:22542–58. Doi: 10.1039/C7TA05609E.
[85] Hawking radiation, the Stefan–Boltzmann law, and unitarization. Phys. Lett. B 2016;754:39–42. Doi: 10.1016/j.physletb.2015.12.076.
[86] Horowitz KAW, Woodhouse M, Lee H, Smestad GP. A bottom-up cost analysis of a high concentration PV module. Aix-Les-Bains, France 2015:100001. https://doi.org/10.1063/1.4931548.
[87] Palfinger G, Bitnar B, Durisch W, Mayor J-C, Grützmacher D, Gobrecht J. Cost estimate of electricity produced by TPV. Semicond. Sci. Technol. 2003;18. https://doi.org/10.1088/0268-1242/18/5/317. S254–61.
[88] Li J, Jiang Y, Liu J, Wu L, Xu N, Zhang Z, et al. A photosynthetically active radiative cooling film. Nat Sustain 2024;7:786–95. https://doi.org/10.1038/s41893-024-01350-6.
[89] López-Ceballos A, del Cañizo C, Antón I, Datas A. Integrating Lithium-Ion and Thermal Batteries with Heat Pumps for Enhanced Photovoltaic Self-Consumption 2024. Doi: 10.2139/ssrn.4743029.
[90] Maisanam AKS, Biswas A, Sharma KK. An innovative framework for electrical energy storage system selection for remote area electrification with renewable energy system: Case of a remote village in India. J Renew Sustain Energy 2020;12:024101. https://doi.org/10.1063/1.5126690.
[91] Sabihuddin S, Kiprakis AE, Mueller M. A Numerical and Graphical Review of Energy Storage Technologies. Energies 2015;8:172–216. https://doi.org/10.3390/en8010172.
[92] Ben Elghali S, Outbib R, Benbouzid M. Selecting and optimal sizing of hybridized energy storage systems for tidal energy integration into power grid. J. Mod Power Syst. Clean Energy 2019;7:113–22. https://doi.org/10.1007/s40565-018-0442-0.
[93] Nikolaidis P, Poullikkas A. Cost metrics of electrical energy storage technologies in potential power system operations. Sustain Energy Technol Assess 2018;25:43–59. https://doi.org/10.1016/j.seta.2017.12.001.
[94] Xu B, Li P, Chan C. Application of phase change materials for thermal energy storage in concentrated solar thermal power plants: a review to recent developments. Appl. Energy 2015;160:286–307. https://doi.org/10.1016/j.apenergy.2015.09.016.
[95] Kapila S, Oni AO, Kumar A. The development of techno-economic models for large-scale energy storage systems. Energy 2017;140:656–72. https://doi.org/10.1016/j.energy.2017.08.117.
[96] Electric Energy Storage Technology Options. A white paper primer on applications, costs, and Benefits. EPRI: Palo Alto, CA; 2010.
[97] Berrada A, Emrani A, Ameur A. Life-cycle assessment of gravity energy storage systems for large-scale application. J Energy Storage 2021;40:102825. https://doi.org/10.1016/j.est.2021.102825.
[98] Jülch V. Comparison of electricity storage options using levelized cost of storage (LCOS) method. Appl. Energy 2016;183:1594–606. https://doi.org/10.1016/j.apenergy.2016.08.165.
[99] Nadeem F, Hussain SMS, Tiwari PK, Goswami AK, Ustun TS. Comparative Review of Energy Storage Systems, their Roles, and Impacts on Future Power Systems. IEEE Access 2019;7:4555–85. https://doi.org/10.1109/ACCESS.2018.2888497.
[100] Xu Y, Pei J, Cui L, Liu P, Ma T. The Levelized cost of Storage of Electrochemical Energy Storage Technologies in China. Front. Energy Res. 2022;10. https://doi.org/10.3389/fenrg.2022.873800.
[101] Linssen J, Stenzel P, Fleer J. Techno-economic analysis of photovoltaic battery systems and the influence of different consumer load profiles. Appl. Energy 2017;185:2019–25. https://doi.org/10.1016/j.apenergy.2015.11.088.
[102] Mongird, Kendall, Viswanathan, Vilayanur V., Balducci, Patrick J., Alam, Md Jan E., Fotedar, Vanshika, Koritarov, V. S., & Hadjerioua, Boualem (2019). Energy Storage Technology and Cost Characterization Report. Doi: 10.2172/157348.
[103] Brinsmead, T.S., Graham, P., Hayward, J., Ratnam, E.L., Reedman, L. (2015). Future Energy Storage Trends: An Assessment of the Economic Viability, Potential Uptake and Impacts of Electrical Energy Storage on the NEM 2015–2035. CSIRO, Australia. Report No. EP155039.